

Piezo-Electroreflectance in Ge, GaAs, and Si†

FRED H. POLLAK AND MANUEL CARDONA*

Physics Department, Brown University, Providence, Rhode Island

(Received 4 December 1967)

We have investigated the effect of static uniaxial compression along the [001], [110], and [111] directions on the E_0 , $E_0+\Delta_0$, E_1 , and $E_1+\Delta_1$ electroreflectance peaks of Ge and GaAs, and the E_0' electroreflectance peaks of Si. From the stress-induced splittings and shifts of the E_0 , $E_0+\Delta_0$ peaks of Ge and GaAs, the hydrostatic and shear deformation potentials of the $\mathbf{k}=0$ valence-band maximum have been determined. We have also observed a nonlinear stress dependence of the energies of these peaks, which is caused by the stress-induced coupling between the upper stress-split valence band and the spin-orbit split band. A theory for the stress-induced variations in intensity caused by this interaction will be presented and compared with the experimental results. The hydrostatic and shear deformation potentials of the Δ_1 -conduction and Δ_3 -valence bands of Ge and GaAs have been determined from the stress dependence of the E_1 and $E_1+\Delta_1$ peaks of these materials. We have attributed the observed stress-induced changes in intensity of these peaks to the intraband splitting of the Δ_3 -orbital valence bands. The experimental results are compared with our theoretical calculations. The stress dependence of the E_0' electroreflectance peaks of Si for [001] stress seems to indicate that [100] critical points are responsible for this structure. However, we have also observed large polarization-dependent intensity changes for [111] stress, which we have not been able to explain on the basis of the above assignment.

I. INTRODUCTION

THE application of a uniaxial stress to a semiconductor produces a strain which reduces the symmetry of the material and results in significant changes in the electronic energy bands.¹ Some of these changes can be determined² from a study of the stress-induced variation of the structure in the normal-incidence optical spectrum, which is attributed to direct interband transitions at certain critical points in the Brillouin zone (BZ). From an analysis of these changes, including polarization and intensity effects, as a function of the magnitude and direction of the applied stress, it is possible to measure deformation potentials and, in principle, to determine the symmetry of the point (or points) in the BZ responsible for the structure.

Recently, several modulation techniques³⁻⁶ have been developed which greatly increase the resolution of optical spectra and enhance critical-point structure with respect to structureless background. One of these methods, electroreflectance at a semiconductor-electrolyte interface,⁶ is particularly suited for an investigation of the effects of uniaxial stress on the energy bands of a semiconductor. The spectra obtained by this technique are often sharper than those obtained from piezoreflec-

tance,⁴ particularly for transitions above the direct edge. The Seraphin technique of electroreflectance³ [the electric field is applied by making the sample one of the plates of a capacitor with a transparent dielectric (Saran Wrap) and a transparent conducting coating (SnO_2) as the other electrode] has the disadvantage that the dielectric material may not remain in uniform contact with the sample surface when the sample is elastically deformed by the stress. Also birefringence in the transparent dielectric due to built-in or applied stress makes measurements with polarized light rather unreliable.

In this paper we report measurements of the effects of static uniaxial compression along the [001], [110], and [111] directions on the E_0 , $E_0+\Delta_0$, E_1 , and $E_1+\Delta_1$ electroreflectance peaks of Ge and GaAs and the E_0' electroreflectance peaks of Si. From the stress-induced splittings and shifts of the E_0 and $E_0+\Delta_0$ peaks (lowest direct gaps at $\mathbf{k}=0$) of Ge and GaAs the hydrostatic and shear deformation potentials of the highest valence-band maximum have been determined.⁷ The shear deformation potentials (b and d) of Ge have been determined by a number of other techniques^{5,8-11} but the values of these quantities obtained by the different methods deviate more than seems possible to ascribe to experimental uncertainties. Hence, we have undertaken another independent investigation of these quantities. The values of b and d for GaAs represent the first determination of the parameters for this material.¹² We have also observed a nonlinear stress dependence of these transitions, which is caused by the stress-induced

† Work supported by the National Aeronautics and Space Administration and the National Science Foundation.

* A. P. Sloan Research Fellow.

¹ I. Goroff and L. Kleinman, *Phys. Rev.* **132**, 1080 (1963).

² U. Gerhardt, *Phys. Rev. Letters* **15**, 401 (1965); *Phys. Status Solidi* **11**, 801 (1965).

³ B. O. Seraphin and R. B. Hess, *Phys. Rev. Letters* **14**, 138 (1965); B. O. Seraphin, R. B. Hess, and N. Bottka, *J. Appl. Phys.* **36**, 2242 (1965); B. O. Seraphin, *Proc. Phys. Soc. (London)* **87**, 239 (1966).

⁴ W. E. Engeler, H. Fritzsche, M. Garfinkel, and J. J. Tiemann, *Phys. Rev. Letters* **14**, 1069 (1965); M. Garfinkel, J. J. Tiemann, and W. E. Engeler, *Phys. Rev.* **148**, 695 (1966).

⁵ I. Balslev, *Phys. Rev.* **143**, 636 (1966).

⁶ M. Cardona, K. L. Shaklee, and F. H. Pollak, *Phys. Rev.* **154**, 696 (1967); M. Cardona, F. H. Pollak, and K. L. Shaklee, *J. Phys. Soc. Japan Suppl.* **21**, 89 (1966).

⁷ A. P. Smith III, M. Cardona, and F. H. Pollak, *Bull. Am. Phys. Soc.* **12**, 101 (1967).

⁸ J. J. Hall, *Phys. Rev.* **128**, 68 (1962).

⁹ A. M. Glass, *Can. J. Phys.* **43**, 12 (1965).

¹⁰ J. C. Hensel, *Solid State Commun.* **4**, 231 (1966).

¹¹ D. H. Dickey and J. O. Dimmock, *J. Phys. Chem. Solids* **28**, 529 (1967).

¹² F. H. Pollak, M. Cardona, and K. L. Shaklee, *Phys. Rev. Letters* **16**, 942 (1966).

coupling between the upper stress-split valence band and the spin-orbit split band. The results are similar to those obtained by Bhargava and Nathan¹³ from the effect of stress on the luminescence spectrum of GaAs.

For transitions at $\mathbf{k} \neq 0$ the application of a uniaxial stress \mathbf{X} can cause two effects: (1) the removal of the equivalence of critical points whose \mathbf{k} vectors do not have equal projections onto the stress direction (interband splitting) and (2) the splitting of doubly degenerate orbital bands whose \mathbf{k} vectors are not parallel to \mathbf{X} (intra-band splitting). Intra-band splitting is difficult to observe in Ge and GaAs since the orbital degeneracy is removed in the unstressed material by the spin-orbit splitting and hence the effect of the stress on the energy eigenvalues is of second order in the ratio α of the orbital to spin-orbit splitting. However, an effect of the first order appears in the wave functions of the "degenerate" bands and hence in the matrix elements for optical transitions.¹⁴ We have observed both intra- and interband splittings of the E_1 and $E_1 + \Delta_1$ electroreflectance peaks of Ge and GaAs and the stress-induced changes in intensity due to the interband splitting of the Δ_3 -orbital valence bands.

We have also investigated the effect of compressive stress on the E_0' peaks of Si. For stress parallel to [001] we have observed splittings consistent with [100] critical points.² Stress along [111] produces no splittings but does cause large polarization-dependent intensity changes. The effects of [110] stress depend not only on the direction of the polarization relative to the stress axis but also on the reflecting face; [110] and [001] faces have been studied.

II. EXPERIMENTAL DETAILS

A. Stress Arrangement

The samples used were aligned by x-ray diffraction to better than 1° and cut to dimensions of approximately $25 \times 1.2 \times 1.0$ mm. The narrow face was mechanically polished and etched. After electrical contacts were applied to the samples they were mounted in the stress frame¹⁵ shown in Fig. 1. The parts of the stress frame were machined from stainless steel and the pistons and frame were polished and fitted together. A force applied upwards on the pull rod is transferred by means of the pull frame to the lower piston, which is movable, to give a compressive stress. The ends of the sample are cemented with Hysol epoxy resin into brass cups placed in thin nylon cups, which act as gaskets, and tightly fitted into the ends of the pistons. Rotation of the pistons while the epoxy is drying enables one to achieve excellent alignment of the sample. In order to minimize any possible bending effects the samples are mounted so that the light is incident on the narrow face.

¹³ R. N. Bhargava and M. I. Nathan, Phys. Rev. **161**, 695 (1967).

¹⁴ M. Cardona and F. H. Pollak, Bull. Am. Phys. Soc. **12**, 101 (1967).

¹⁵ M. Cuevas and H. Fritzsche, Phys. Rev. **137**, A1847 (1965).

The details of the brass cups used are shown in the right-hand corner of Fig. 1. If the solder contact on the sample were to touch the brass cup a short circuit between the sample and the electrolyte would result since the entire frame is immersed in the electrolyte. This short circuit would bypass the blocking contact of the semiconductor-electrolyte interface, which produces the electroreflectance effect. In order to avoid this difficulty the brass cups, which are $\frac{1}{4}$ in. in diam and $\frac{1}{2}$ in. in length, have a $\frac{3}{16}$ -in. hole drilled in them to a depth of $\frac{7}{16}$ in. This hole is then filled with epoxy to a depth of $\frac{3}{8}$ in. and a brass plug of diameter slightly under $\frac{1}{8}$ in. and $\frac{1}{4}$ in. long is then epoxied into this hole and allowed to dry. The hole to accommodate the sample is then drilled into the brass plug and when the sample is mounted a small amount of epoxy is placed around the region where the sample enters the brass plug so that it is insulated from the electrolyte. The purpose of the brass plug is to distribute the force applied to the sample over a larger area since the epoxy itself would yield somewhat if the sample were mounted directly into it.

The pull rod is connected to a lever arm by means of a T-shaped connector, the arms of the T riding in needle bearings such that the pull rod remains vertical as the lever arm moves about the fulcrum. The other end of the lever arm, which has a 10:1 ratio, is connected to a spring by means of a yoke. The yoke is also connected to the lever arm by means of needle bearings so that it too remains vertical when the lever arm moves. The stress is applied by turning the knob so that the spring is elongated. The extension of the spring is measured by a Schaevitz linear variable differential transformer (LVDT) mounted inside the spring.¹⁶ A matched LVDT is mounted on a micrometer, divided in ten-thousandths of an inch, outside the system. The two LVDT's are

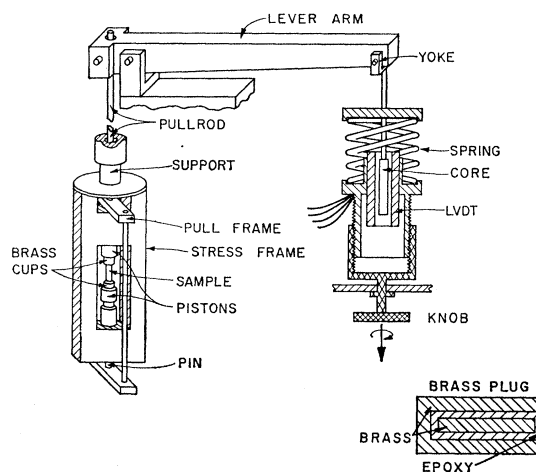


FIG. 1. Stress apparatus used for piezo-electroreflectance measurements.

¹⁶ F. H. Pollak, Phys. Rev. **138**, A618 (1965); A. Feldman, *ibid.* **150**, 748 (1966).

connected as the two arms of an ac bridge, the null being detected by a vacuum-tube voltmeter. The output voltage per displacement of the LVDT's can be matched to about 0.2%. The spring is calibrated by removing it from the assembly and hanging weights on it.

B. Optics and Electronics

Monochromatic light was produced with a Bausch & Lomb 50-cm monochromator.

An HR-8 Princeton Applied Research lock-in amplifier was used throughout our investigation.

We recorded the ratio $\Delta R/R$ of the reflectivity modulation to the reflectivity as a function of wavelength. In order to obtain this parameter directly when a photomultiplier was used as a detector we applied the dc output from the photomultiplier to a servomechanism which acts on a helipot voltage divider and sets the high voltage applied to the photomultiplier. The high voltage is varied so as to keep the dc output voltage constant and hence the ac signal from the lock-in amplifier is proportional to the ratio $\Delta R/R$. The value of $\Delta R/R$ is then obtained by dividing the signal from the amplifier by the value of the constant dc voltage.⁶ This scheme cannot be employed for the E_0 and $E_0 + \Delta_0$ peaks of Ge since no photomultipliers are available which operate in this wavelength region. The electroreflectance signal of these peaks was detected with a PbS photoconductive Kodak Ektron cell. In order to obtain a signal proportional to R a small portion of the incident light was chopped at 13 cps and measured with a separate lock-in amplifier. The ratio of the two signals is proportional to $\Delta R/R$.

C. Electrolytic Cell

Except for the investigation of the E_0 and $E_0 + \Delta_0$ peaks of Ge the electrolytic cell used was similar to the one already described.⁶ In the infrared region ($\approx 1.2 \mu$) water absorbs strongly so that in order to perform measurements in this region the sample must be placed close to the window of the electrolytic cell so as to reduce the water absorption while still maintaining a thin layer of electrolyte (0.1 mm) capable of producing the field modulation.¹⁷ In order to accomplish this with the sample mounted in the stress frame (see Fig. 1) a special electrolytic cell was constructed with a quartz window which extended inward about $\frac{1}{2}$ in. In this manner the window could be placed protruding inside the stressing frame quite close to the sample. The window was constructed so that the face next to the sample is at an angle of about 6° with the front face thus reducing to less than 10% the light reflected from the front face into the detector. The depolarizing effects of $\frac{1}{2}$ in. length of quartz window were found to be negligible. The data reported here were all taken at room temperature.

¹⁷ M. Cardona, K. L. Shaklee, and F. H. Pollak, Phys. Letters 23, 37 (1966).

D. Sample Characteristics

All samples were cut from a single ingot of the respective material. Sample characteristics, dc bias and ac modulating voltages are listed in Table I. The sign of the dc bias refers to the polarity of the sample relative to the platinum electrode.

III. COMPARISON OF EXPERIMENTAL RESULTS AND THEORY

A. Transitions at $k=0$: E_0 and $E_0 + \Delta_0$ Peaks

Without strain or spin-orbit splitting the valence-band edge at $k=0$ in a diamond- or zinc blende-type material is a sixfold degenerate multiplet with orbital symmetry $\Gamma_{25'}$ (diamond) or Γ_{15} (zinc blende). The spin-orbit interaction lifts this degeneracy into a fourfold $p_{3/2}$ multiplet ($J = \frac{3}{2}$, $m_J = \pm \frac{3}{2}, \pm \frac{1}{2}$ in spherical notation) and a $p_{1/2}$ multiplet ($J = \frac{1}{2}$, $m_J = \pm \frac{1}{2}$) as shown in Fig. 2. The application of a uniaxial stress splits the $p_{3/2}$ multiplet and also, because of the hydrostatic pressure component of the strain, shifts (1) the "center of gravity" of the $p_{3/2}$ multiplet and (2) the $p_{1/2}$ band relative to the conduction band ($\Gamma_{2'}$ for Ge and Γ_1 for GaAs) as illustrated schematically in Fig. 2. The three valence bands have been labeled v_1 , v_2 , and v_3 . The transitions between these valence bands and the $\Gamma_{2'}$ (Γ_1) conduction band have been labeled $E_0(1)$, $E_0(2)$, and $E_0 + \Delta_0$, respectively. From the splittings and shifts of the various bands we have determined the hydrostatic and shear deformation potentials of the valence-band edge. The stress-induced coupling of v_1 and v_3 produces (a) a stress-dependent variation in the intensities of $E_0(1)$ and $E_0 + \Delta_0$ and (b) a nonlinear stress dependence of the energies of these transitions.

It has been shown that the orbital-strain Hamiltonian \mathcal{H}_ϵ for a given band at $k=0$ can be written as¹⁸⁻²⁰

$$\mathcal{H}_\epsilon(i) = -a^{(i)}(\epsilon_{xx} + \epsilon_{yy} + \epsilon_{zz}) - 3b^{(i)}[(L_x^2 - \frac{1}{3}L^2)\epsilon_{xx} + \text{c.p.}] - (6d^{(i)}/\sqrt{3})[\{L_x L_y\}\epsilon_{xy} + \text{c.p.}], \quad (1a)$$

where the superscript i is a band index, $\epsilon_{\alpha\beta}$ denotes the components of the strain tensor, L is the angular-momentum operator, c.p. denotes cyclic permutations with respect to the indices, x , y , and z , and the quantities in the curly brackets indicate the symmetrized product: $\{L_x L_y\} = \frac{1}{2}(L_x L_y + L_y L_x)$. The parameter $a^{(i)}$ is the hydrostatic pressure-deformation potential for a given band. Since, experimentally, we can measure only the energy difference between two bands, it is only possible to determine the relative hydrostatic-pressure coefficient between the $\Gamma_{2'}$ (Γ_1) conduction band and the $\Gamma_{25'}$ (Γ_{15}) valence bands. The quantities $b^{(i)}$ and $d^{(i)}$ are uniaxial-

¹⁸ G. E. Picus and G. L. Bir, Fiz. Tverd. Tela 1, 154 (1959); 1, 1642 (1959); G. E. Picus, *ibid.* 6, 324 (1963) [English transl.: Soviet Phys.—Solid State 1, 136 (1959); 1, 1502 (1960); 6 261 (1964)]; G. E. Picus, Zh. Eksperim. i Teor. Fiz. 41, 1507 (1961) [English transl.: Soviet Phys.—JETP 14, 1075 (1962)].

¹⁹ H. Hasegawa, Phys. Rev. 129, 1029 (1963).

²⁰ J. C. Hensel and G. Feher, Phys. Rev. 129, 1041 (1963).

TABLE I. Sample characteristics, dc bias (V_{dc}), and ac modulating voltage (V_{ac}). The sign of the dc bias refers to the polarity of the sample relative to the platinum electrode.

Material	Type	Carrier concentration (cm ⁻³)	V_{dc} (V)	V_{ac} (V rms)
Ge	<i>p</i>	2×10^{16}	-0.25	0.25
GaAs	<i>n</i>	6×10^{15}	-0.75	1.25
Si	<i>n</i>	1×10^{16}	+3.00	3.00

deformation potentials appropriate to strains of tetragonal and rhombohedral symmetries, respectively. The symbols b and d without superscripts will be used for the uniaxial-deformation potentials of the $\Gamma_{25'}$ (Γ_{15}) valence bands.

The total Hamiltonian is then given by

$$\mathcal{H}^{(i)} = \mathcal{H}_{s.o.} + \mathcal{H}_e^{(i)}, \quad (1b)$$

where $\mathcal{H}_{s.o.}$ is the spin-orbit Hamiltonian in the absence of stress. Stress contributions to the spin-orbit Hamiltonian will not be considered at this point.

1. Stress Parallel to [001]

For a [001] stress the strain components are

$$\begin{aligned} \epsilon_{zz} &= S_{11}X, \\ \epsilon_{xx} &= \epsilon_{yy} = S_{12}X, \\ \epsilon_{xy} &= \epsilon_{xz} = \epsilon_{yz} = 0, \end{aligned}$$

where S_{11} and S_{12} are elastic compliance constants.²¹ The strain Hamiltonian for the energy difference between the $\Gamma_{25'}$ (Γ_{15}) and the $\Gamma_{2'}$ (Γ_1) band becomes

$$\mathcal{H}_e = -a(S_{11} + 2S_{12})X - 3b(S_{11} - S_{12})X(L_z^2 - \frac{1}{3}\mathbf{L}^2), \quad (2a)$$

$$\mathcal{H}_e = -\delta E_H - \frac{2}{3}\delta E_{001}(L_x^2 - \frac{1}{3}\mathbf{L}^2), \quad (2b)$$

where $\delta E_H = a(S_{11} + 2S_{12})X = (\partial E_g / \partial P) \times P$ is the shift of the gap E_g , due to the hydrostatic component of the strain, and $\delta E_{001} = 2b(S_{11} - S_{12})X$ is the linear splitting of the $p_{3/2}$ multiplet.

The wave functions for the valence-band states will be taken in the (J, m_J) representations in which $\mathcal{H}_{s.o.}$ is diagonal. Referred to the [001] direction the unperturbed wave functions of the valence and conduction

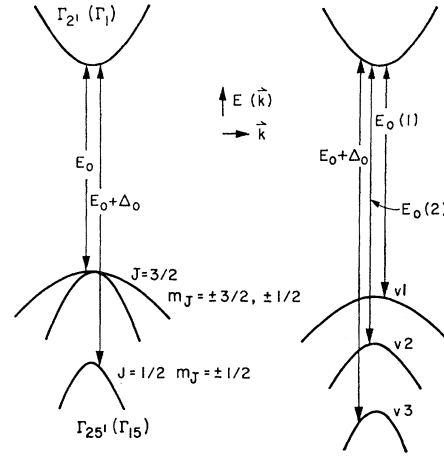


FIG. 2. The left side shows the valence bands ($J = \frac{3}{2}$, $m_J = \pm \frac{3}{2}$, $\pm \frac{1}{2}$, and $J = \frac{1}{2}$, $m_J = \pm \frac{1}{2}$ in spherical notation) and lowest conduction band in unstressed Ge and GaAs near $\mathbf{k}=0$. The right side shows the effect of compressive stress on the bands and the allowed transitions.

bands are given by²²

$$\begin{aligned} u_{v2,0} &= |\frac{3}{2}, \frac{3}{2}\rangle_{001} = |(\frac{1}{2})^{1/2}(X+iY)\uparrow\rangle, \\ u_{v1,0} &= |\frac{3}{2}, \frac{1}{2}\rangle_{001} = |(\frac{1}{6})^{1/2}[2Z\uparrow - (X+iY)\downarrow]\rangle, \\ u_{v3,0} &= |\frac{1}{2}, \frac{1}{2}\rangle_{001} = |(\frac{1}{3})^{1/2}[Z\uparrow + (X+iY)\downarrow]\rangle, \\ u_{c,0} &= |S\uparrow\rangle, \end{aligned} \quad (3)$$

where \uparrow and \downarrow indicate spin up and spin down referred to the stress axis, respectively. The symmetry properties of the wave functions of Ge and GaAs are identical under the point group of the tetrahedron; differences arise for the other point group operations of the cube. Since the strain Hamiltonian of Eq. (1) has even parity we can neglect these differences. In Eq. (3) X , Y , Z are the valence-band wave functions which transform as atomic p functions under the operations of the group of the tetrahedron and S is the conduction-band wave function which transforms as an atomic s function under the same operations. Only states of positive m_J have been considered since the stress does not remove the Kramers degeneracy of each state.

From Eqs. (2b) and (3) the Hamiltonian matrix for the valence bands can be written as

$$\begin{vmatrix} |\frac{3}{2}, \frac{3}{2}\rangle_{001} & |\frac{3}{2}, \frac{1}{2}\rangle_{001} & |\frac{1}{2}, \frac{1}{2}\rangle_{001} \\ \frac{1}{3}\Delta_0 - \delta E_H - \frac{1}{2}\delta E_{001} & 0 & 0 \\ 0 & \frac{1}{3}\Delta_0 - \delta E_H + \frac{1}{2}\delta E_{001} & \frac{1}{2}\sqrt{2}\delta E_{001} \\ 0 & \frac{1}{2}\sqrt{2}\delta E_{001} & -\frac{2}{3}\Delta_0 - \delta E_H \end{vmatrix}, \quad (4)$$

where Δ_0 is the spin-orbit splitting of the valence bands at $\mathbf{k}=0$ (0.29 eV for Ge and 0.34 eV for GaAs).

²¹ The values of the elastic compliance constants of Ge and GaAs are given, respectively, by M. E. Fine, J. Appl. Phys. **26**, 862 (1955) and O. Madelung, *Physics of III-V Compounds* (John Wiley & Sons, Inc., New York, 1964), p. 345.

Diagonalizing the above Hamiltonian we find, for the change in the energy difference between the con-

²² See, e.g., C. Kittel, *Quantum Theory of Solids* (J. Wiley & Sons, Inc., New York, 1963), p. 282.

duction and valence bands at $\mathbf{k}=0$,

$$\begin{aligned}\Delta(E_c - E_{v2}) &= -\frac{1}{3}\Delta_0 + \delta E_H + \frac{1}{2}\delta E_{001}, \\ \Delta(E_c - E_{v1}) &= \frac{1}{6}\Delta_0 + \delta E_H - \frac{1}{4}\delta E_{001} \\ &\quad - \frac{1}{2}[\Delta_0^2 + \Delta_0\delta E_{001} + (9/4)(\delta E_{001})^2]^{1/2}, \\ \Delta(E_c - E_{v3}) &= \frac{1}{6}\Delta_0 + \delta E_H - \frac{1}{4}\delta E_{001} \\ &\quad + \frac{1}{2}[\Delta_0^2 + \Delta_0\delta E_{001} + (9/4)(\delta E_{001})^2]^{1/2}.\end{aligned}\quad (5)$$

For $\delta E_{001} \ll \Delta_0$ Eq. (5) can be expanded in powers of $\delta E_{001}/\Delta_0$ to give

$$\begin{aligned}\Delta(E_c - E_{v2}) &= -\frac{1}{3}\Delta_0 + \delta E_H + \frac{1}{2}\delta E_{001}, \\ \Delta(E_c - E_{v1}) &= -\frac{1}{3}\Delta_0 + \delta E_H - \frac{1}{2}\delta E_{001} - \frac{1}{2}(\delta E_{001})^2/\Delta_0 + \dots, \\ \Delta(E_c - E_{v3}) &= +\frac{2}{3}\Delta_0 + \delta E_H + \frac{1}{2}(\delta E_{001})^2/\Delta_0 + \dots.\end{aligned}\quad (6)$$

It should be noted that since the state $|\frac{3}{2}, \frac{3}{2}\rangle$ is not coupled by the stress to the other two valence bands it has a linear stress dependence while the states with $m_J = \frac{1}{2}$ have a nonlinear stress dependence (repulsion) caused by the off-diagonal terms in Eq. (4).

In Appendix A the wave functions of the three valence band states are listed to first order in \mathbf{X} . From these wave functions the selection rules and relative intensities for transitions to $\Gamma_{2'}$, (Γ_1) have been calculated, as a function of \mathbf{X} , for light polarized parallel and perpendicular to the stress axis. These intensities are given by²³

$$\begin{aligned}I_2^{\parallel}(\mathbf{X}) &= 0, & I_2^{\perp}(\mathbf{X}) &= I_2^{\perp}(0), \\ I_1^{\parallel}(\mathbf{X}) &= I_1^{\parallel}(0)(1 + \alpha_0), & I_1^{\perp}(\mathbf{X}) &= I_1^{\perp}(0)(1 - 2\alpha_0), \\ I_3^{\parallel}(\mathbf{X}) &= I_3^{\parallel}(0)(1 - 2\alpha_0), & I_3^{\perp}(\mathbf{X}) &= I_3^{\perp}(0)(1 + \alpha_0),\end{aligned}\quad (7)$$

where subscripts 1, 2, and 3 refer to transitions from v_1 , v_2 , and v_3 , respectively, to the conduction band, \parallel and \perp indicate light polarized parallel and perpendicular to the stress axis, respectively, and $\alpha_0 = \delta E_{001}/\Delta_0$. Note that for states of $m_J = \frac{3}{2}$ only the perpendicular-polarization transition occurs.

Shown in Figs. 3 and 4 are the electroreflectance spectra of Ge and GaAs, respectively, for zero stress and stress along $[001]$ with the electric-field vector of the incident light polarized parallel and perpendicular to the stress axis. The line shape of the spectra at zero stress for both materials agree with the theory of Aspnes²⁴ for an M_0 transition. For Ge the light was incident on the sample surface normal to $[110]$ ($[110]$ face), while the GaAs the light was incident on a $[100]$ face. The scale of $\Delta R/R$ in Fig. 4 is arbitrary for the reason mentioned in Sec. II B. The E_0 peak has been split by the action of the uniaxial stress: for \perp polarization two transitions are seen, $E_0(1)$ and $E_0(2)$, while for the \parallel polarization only one peak, $E_0(1)$, is observed. For the latter polarization the peaks which appear at higher energies are Franz-Keldysh oscillations and not a splitting; this fact appears clearly when the peaks are

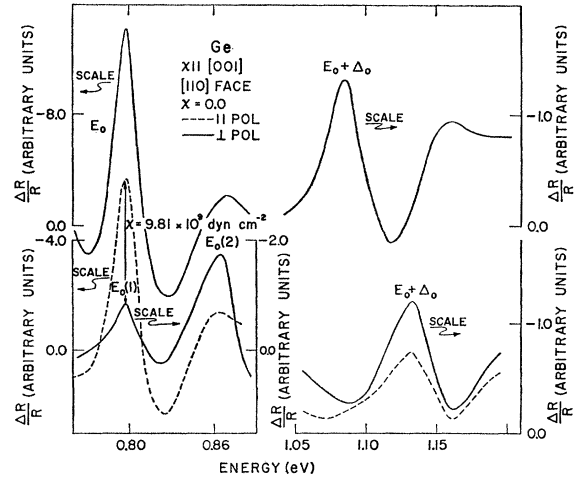


FIG. 3. Electroreflectance spectra of the E_0 and $E_0 + \Delta_0$ peaks of Ge for zero stress and for a stress of 9.81×10^9 dyn cm^{-2} along $[001]$ with light polarized parallel and perpendicular to the stress axis. For zero stress the polarization effects are negligible so that only one polarization direction has been plotted.

tracked as a function of stress. From Eq. (7) we identify $E_0(1)$ as caused by transitions from v_1 to the conduction band, while $E_0(2)$ is due to transitions from v_2 (see Fig. 2). The energy of $E_0(1)$ is the same for both polarization directions. The E_0 peak, in addition to being split, has had its center of gravity shifted to higher energies. The $E_0 + \Delta_0$ peak, which is caused by transitions from v_3 to $\Gamma_{2'}$, (Γ_1), has been shifted to higher energies but not split.

In Figs. 5 and 6 we have plotted the energies of $E_0(1)$, $E_0(2)$, and $E_0 + \Delta_0$ as a function of stress for Ge and GaAs, respectively. The energy of $E_0(2)$ varies linearly with \mathbf{X} while $E_0(1)$, which has a linear stress dependence at low stresses, exhibits a nonlinear be-

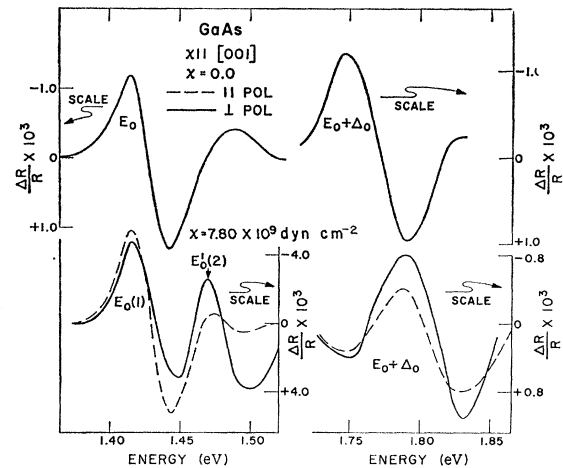


FIG. 4. Electroreflectance spectra of the E_0 and $E_0 + \Delta_0$ peaks of GaAs for zero stress and for a stress of 7.80×10^9 dyn cm^{-2} along $[001]$ with light polarized parallel and perpendicular to the stress axis. For zero stress the polarization effects are negligible, so that only one polarization direction has been plotted.

²³ D. G. Thomas, J. Appl. Phys. **32S**, 2298 (1961).

²⁴ D. Aspnes, Phys. Rev. **147**, 554 (1966); **153**, 972 (1967).

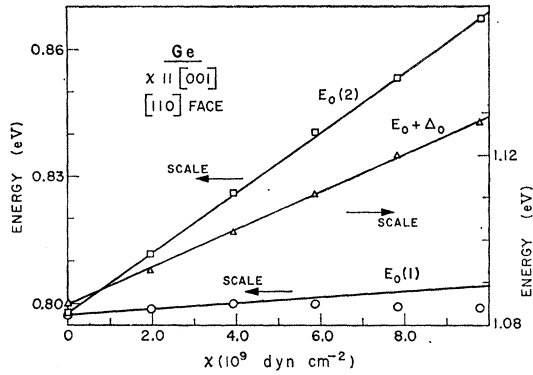


FIG. 5. Energies of the $E_0(1)$, $E_0(2)$, and $E_0 + \Delta_0$ peaks of the electroreflectance spectrum of Ge as a function of uniaxial stress along $[001]$.

havior at high stresses. Listed in Table II²⁵ are the values of the deformation potentials $\partial E_g/\partial P$ and b for Ge and GaAs as determined from Eq. (6) and the experimental data shown in Figs. 5 and 6, respectively. The values of $b^2(S_{11} - S_{12})^2$, which will be used subsequently for comparison with the results of measurements with stress along $[110]$, have also been listed in Table II for these materials. The values of $\partial E_g/\partial P$ have also been determined from the shift of $E_0 + \Delta_0$ and are in good agreement with those deduced from the data for $E_0(1)$ and $E_0(2)$. The experimental error in the determination

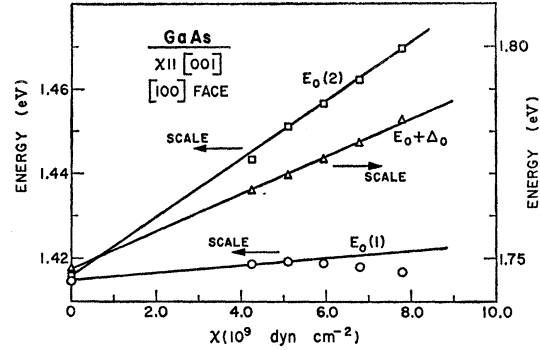


FIG. 6. Energies of the $E_0(1)$, $E_0(2)$, and $E_0 + \Delta_0$ peaks of GaAs as a function of uniaxial stress along $[001]$.

of the stress dependence of $E_0 + \Delta_0$ is larger because of the smaller wavelength shift and the lower signal-to-noise ratio due to the smaller signal for this peak. Because of this larger experimental uncertainty, and the fact that for this peak the nonlinear term is superimposed on a large hydrostatic shift, the nonlinear term was not observed for the $E_0 + \Delta_0$ peak.

Figure 3 reveals that the intensities of the electroreflectance peaks of Ge are in qualitative agreement with theory [Eq. (7)]. Since I_2^1 and I_1^1 of Eq. (7) can only be measured at high stresses, for which the peaks are resolved, the theoretical values of the zero-stress in-

TABLE II. Deformation potentials for Ge and GaAs.

	Ge		GaAs	
	This work	Previous results	This work	Previous results
$\partial E_g/\partial P$ (10^{-6} eV bar $^{-1}$)	$+12.0 \pm 0.5^a$ $+12.5 \pm 0.5^b$ $+12.5 \pm 0.7^c$	$+13 \pm 1^d$ $+13.7 \pm 1.5^e$ $+10.6^f$	$+11.5 \pm 0.5^a$ $+12.0 \pm 0.5^b$ $+11.5 \pm 0.5^c$	$+11.5 \pm 1^d$ $+11.8 \pm 0.6^k$ $+10.5^f$
b (eV)	-2.6 ± 0.2^a	-2.7 ± 0.3^e -2.4 ± 0.2^f -1.8 ± 0.2^g -2.1 ± 0.2^h	-2.0 ± 0.2^a	-1.7 ± 0.2^f -1.96 ± 0.1^k
d (eV)	-4.7 ± 0.3^b	-4.7 ± 0.5^e -4.1 ± 0.4^f -3.7 ± 0.4^g -7.0 ± 1.5^h -6.0 ± 0.6^i	-6.0 ± 0.4^b	-4.4 ± 0.6^f -5.4 ± 0.3^k
$b^2(S_{11} - S_{12})^2$ [10^{-24} (eV cm 2 dyn $^{-1}$) 2]	10.4 ± 1.5^a		9.6 ± 1.0^a	
$\frac{1}{4}d^2S_{44}^2$ [10^{-24} (eV cm 2 dyn $^{-1}$) 2]	12.3 ± 1.6^b		26.4 ± 3.5^b	
$b^2(S_{11} - S_{12})^2 + \frac{1}{4}d^2S_{44}^2$ [10^{-24} (eV cm 2 dyn $^{-1}$) 2]	19.7 ± 3.0^c		30.9 ± 4.5^c	
ϵ_1 (eV)	-4.5 ± 0.4^a	-5.7 ± 0.4^d -5.7 ± 0.3^j	-4.0 ± 0.4^a	
ϵ_2 (eV)	$+5.1 \pm 1.0^{a,b}$	$+5.1 \pm 1.0^i$	$+7.4 \pm 0.7^b$	

^a $[001]$ stress measurements.

^b $[110]$ stress measurements.

^c Reference 9.

^d Reference 5.

^e Reference 10.

^f Reference 13.

^g $[111]$ stress measurements.

^h Reference 25.

ⁱ I. Blaslev, Solid State Commun. **5**, 315 (1967).

^j Reference 8.

^k Reference 12.

²⁵ J. Feinleib, S. Groves, W. Paul, and R. Zallen, Phys. Rev. **131**, 2070 (1963); R. Zallen and W. Paul, *ibid.* **134**, A1628 (1964); **155**, 703 (1967).

tensities (see Appendix A) will be used in the following discussion: In Table III the values of the intensity ratio I_1^{11}/I_1^{\perp} , I_2^{\perp}/I_1^{\perp} , and I_3^{\perp}/I_3^{11} for $X=9.80 \times 10^9$ dyn cm^{-2} as calculated from Eq. (7) and the value of b for Ge listed in Table II are compared to the experimental values taken from Fig. 3. The intensities have been measured peak to peak in order to avoid any errors due to background signals. The theoretical values of I_1^{11}/I_1^{\perp} and I_3^{\perp}/I_3^{11} are in good agreement with experiment. The discrepancy for the ratio I_2^{\perp}/I_1^{\perp} is to be expected since the $E_0(2)$ peak has a much larger lifetime broadening than $E_0(1)$ for perpendicularly polarized light; Fig. 3 indicates that the width of $E_0(2)$ is about twice that of $E_0(1)$. When this fact is introduced into the experimental value of this ratio reasonable agreement is obtained. As shown in Fig. 4 the intensities for GaAs are not in agreement with the theoretical results of Eq. (7): experimentally $I_1^{11}/I_1^{\perp} \approx 1$ and $I_2^{\perp}/I_1^{\perp} \approx 0.7$ as opposed to $I_1^{11}/I_1^{\perp} = 6.2$ and $I_2^{\perp}/I_1^{\perp} = 4.1$ obtained from Eq. (7). We believe the reason for this discrepancy is that the transitions causing this structure take place from the valence band to a shallow donor level rather than to the conduction band. This impurity effect has been observed before in this material.^{6,26} It is believed that the impurity is a donor rather than an acceptor since the stress-induced splittings of the E_0 peak are in agreement with Eq. (6), which would not be the case for an acceptor: An acceptor level has a nonlinear stress shift relative to the valence band and hence $E_0(2)$ would not have a linear stress dependence.

2. Stress Parallel to [111]

For this stress direction the analysis is almost identical to that for the stress along [001]. The strain components are given by

$$\begin{aligned}\epsilon_{xx} = \epsilon_{yy} = \epsilon_{zz} &= (S_{11} + 2S_{12})(\frac{1}{3}X), \\ \epsilon_{xy} = \epsilon_{yz} = \epsilon_{zx} &= (\frac{1}{2}S_{44})(\frac{1}{3}X),\end{aligned}$$

where S_{44} is an elastic compliance constant. The strain

TABLE III. Comparison of the experimental and theoretical values of the intensity ratios I_1^{11}/I_1^{\perp} , I_2^{\perp}/I_1^{\perp} , and I_3^{\perp}/I_3^{11} for the E_0 , $E_0 + \Delta_0$ peaks of Ge.

Stress direction and magnitude		$\frac{I_1^{11}}{I_1^{\perp}}$	$\frac{I_2^{\perp}}{I_1^{\perp}}$	$\frac{I_3^{\perp}}{I_3^{11}}$
[001] Expt.		8.0	1.8	1.6
9.81×10^9 dyn cm^{-2} Theory		8.5	5.2	2.1
[111] Expt.		5.7	2.8	1.9
9.32×10^9 dyn cm^{-2} Theory		6.1	4.1	1.5
[110]{[001] face} Expt.		2.6	1.2	0.9
9.02×10^9 dyn cm^{-2} Theory		14.2	8.4	1.5
[110]{[110] face} Expt.		1.7	1.3	0.9
9.68×10^9 dyn cm^{-2} Theory		4.3	3.3	1.8

²⁶ M. Cardona and W. Paul, J. Phys. Chem. Solids 17, 138 (1960).

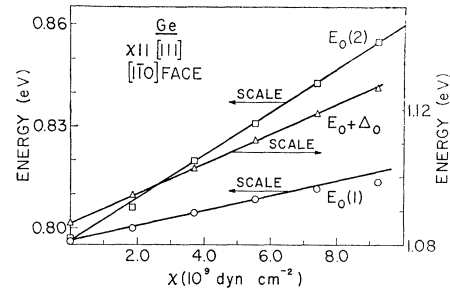


Fig. 7. Energies of the $E_0(1)$, $E_0(2)$, and $E_0 + \Delta_0$ peaks of Ge as a function of uniaxial stress along [111].

Hamiltonian of Eq. (1) now has the form

$$\mathcal{H}_\epsilon = -a(S_{11} + 2S_{12})X - (6d/\sqrt{3}) \times [\{L_x L_y\} + \{L_y L_z\} + \{L_z L_x\}] (\frac{1}{2}S_{44})(\frac{1}{3}X). \quad (8)$$

The problem of diagonalizing \mathcal{H}_ϵ can be simplified considerably if we make a transformation such that the [111] direction becomes the z axis. The transformed wave functions are listed in Appendix A. Under this rotation the Hamiltonian matrix for this stress direction has the same form as the matrix for along the [001] direction, Eq. (4), with the quantity $\delta E_{111} = (d/\sqrt{3})S_{44}X$ replacing δE_{001} . Therefore, from Eq. (6) we may write for the energy change between the conduction and valence bands:

$$\begin{aligned}\Delta(E_c - E_{v2}) &= -\frac{1}{3}\Delta_0 + \delta E_H + \frac{1}{2}\delta E_{111}, \\ \Delta(E_c - E_{v1}) &= -\frac{1}{3}\Delta_0 + \delta E_H - \frac{1}{2}\delta E_{111} - \frac{1}{2}(\delta E_{111})^2/\Delta_0 + \dots \\ \Delta(E_c - E_{v3}) &= +\frac{2}{3}\Delta_0 + \delta E_H + \frac{1}{2}(\delta E_{111})^2/\Delta_0 + \dots.\end{aligned} \quad (9)$$

In Figs. 7 and 8 are shown the energies of $E_0(1)$, $E_0(2)$, and $E_0 + \Delta_0$ as a function of [111] stress for Ge and GaAs, respectively. In a manner similar to that already described for the case of [001] stress the deformation potentials $\partial E_g/\partial P$ and d have been determined from the experimental data. These are listed in Table II in addition to the values of $\frac{1}{4}d^2S_{44}^2$ which will be used for a comparison with the results for [110] stress.

The intensities of the E_0 and $E_0 + \Delta_0$ lines as a function of stress are given by Eq. (7) with α_0 replaced by $\alpha_0' = \delta E_{111}/\Delta_0$. The agreement between these calculated intensities and the experimentally observed ones for Ge is similar to that discussed for [001] stress. The calculated and observed intensities are listed in Table III for $X = 9.23 \times 10^9$ dyn cm^{-2} .

3. Stress Parallel to [110]

For the case of stress parallel to [001] or [111] the choice of the quantization axis along the stress direction led to a simple form for the Hamiltonian and the wave

functions. This choice preserved m_J as a good quantum number and hence led to well-defined selection rules and an easy identification of states. However, when stress is applied to an axis of lower symmetry such as the [110] axis, the situation is considerably more complicated.

For stress along this axis we have

$$\begin{aligned}\epsilon_{xx} &= \epsilon_{yy} = (S_{11} + S_{12})\left(\frac{1}{2}X\right), \\ \epsilon_{zz} &= S_{12}X, \\ \epsilon_{yx} &= \left(\frac{1}{3}S_{44}\right)\left(\frac{1}{2}X\right), \\ \epsilon_{xz} &= \epsilon_{yz} = 0.\end{aligned}$$

If we rotate \mathbf{L} according to the transformation

$$\begin{aligned}\tilde{L}_x &= L_x, \\ \tilde{L}_y &= \frac{1}{2}\sqrt{2}[L_x - L_y], \\ \tilde{L}_z &= \frac{1}{2}\sqrt{2}[L_x + L_y],\end{aligned}\quad (10)$$

the strain Hamiltonian of Eq. (1) becomes

$$\mathcal{H}_\epsilon[110] = -\delta E_H + \frac{1}{4}\delta E_{001}[3(\tilde{L}_y)^2 - (\tilde{L}_z)^2] - \frac{3}{4}\delta E_{111}[(\tilde{L}_z)^2 - (\tilde{L}_x)^2]. \quad (11)$$

The wave functions referred to the [110] direction as the z axis are listed in Appendix A.

Using these wave functions the Hamiltonian matrix becomes

$$\begin{vmatrix} \left| \frac{3}{2}, \frac{3}{2} \right\rangle_{110} & \left| \frac{3}{2}, -\frac{1}{2} \right\rangle_{110} & \left| \frac{1}{2}, -\frac{1}{2} \right\rangle_{110} \\ \frac{1}{3}\Delta_0 - \delta E_H & -\frac{1}{8}\sqrt{3}(\delta E_{001} - \delta E_{111}) & \frac{1}{8}\sqrt{6}(\delta E_{001} - \delta E_{111}) \\ -\frac{1}{8}(\delta E_{001} + 3\delta E_{111}) & \frac{1}{3}\Delta_0 - \delta E_H + \frac{1}{8}(\delta E_{001} + 3\delta E_{111}) & \frac{1}{8}\sqrt{2}(\delta E_{001} + 3\delta E_{111}) \\ -\frac{1}{8}\sqrt{3}(\delta E_{001} - \delta E_{111}) & \frac{1}{8}\sqrt{2}(\delta E_{001} + 3\delta E_{111}) & -\frac{2}{3}\Delta_0 - \delta E_H \end{vmatrix}, \quad (12)$$

with an identical matrix for the states $\left| \frac{3}{2}, -\frac{3}{2} \right\rangle_{110}$, $\left| \frac{3}{2}, \frac{1}{2} \right\rangle_{110}$, and $\left| \frac{1}{2}, \frac{1}{2} \right\rangle_{110}$. The above Hamiltonian is not diagonal in the representation referred to the [110] direction as the z axis with the consequence that $\pm m_J$ is no longer a good quantum number and in general the strain-split states will consist of mixtures of basis function for $m_J \pm \frac{3}{2}$ and $m_J = \pm \frac{1}{2}$.

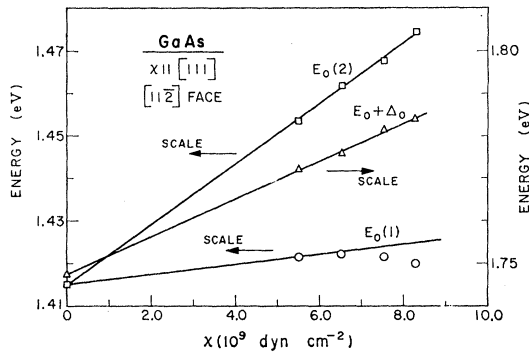


FIG. 8. Energies of the $E_0(1)$, $E_0(2)$, and $E_0 + \Delta_0$ peaks of GaAs as a function of uniaxial stress along [111].

In the case that $\delta E_{001} = \delta E_{111}$ (equal band splitting under applied stress along [001] or [111]) the above matrix would have the same form as the case of \mathbf{X} parallel to [001] or [111]. In fact, under this condition, the band splitting becomes isotropic and the Hamiltonian matrix has the form of Eq. (4) for any direction of

stress. As can be seen from Figs. 5–8 this is only approximately the case for Ge and GaAs.

The eigenvalues of Eq. (12) can be found by first diagonalizing the 4×4 matrix in the upper-left-hand corner and then including the effects of the $\left| \frac{1}{2}, -\frac{1}{2} \right\rangle_{110}$ band by second-order perturbation theory. We obtain

$$\begin{aligned}\Delta(E_c - E_{e2}) &= -\frac{1}{3}\Delta_0 + \delta E_H + \frac{1}{4}[(\delta E_{001})^2 + 3(\delta E_{111})^2]^{1/2} \\ &\quad - \frac{3}{32}(\delta E_{001} - \delta E_{111})^2/\Delta_0 + \dots, \\ \Delta(E_c - E_{e1}) &= -\frac{1}{3}\Delta_0 + \delta E_H - \frac{1}{4}[(\delta E_{001})^2 + 3(\delta E_{111})^2]^{1/2} \\ &\quad - \frac{1}{4}(\delta E_{001} + 3\delta E_{111})^2/\Delta_0 + \dots, \\ \Delta(E_c - E_{e3}) &= \frac{2}{3}\Delta_0 + \delta E_H + \frac{1}{4}[(\delta E_{001})^2 + 3(\delta E_{111})^2]^{1/2} \\ &\quad + \frac{3}{32}(\delta E_{001} - \delta E_{111})^2/\Delta_0 + \dots,\end{aligned}\quad (13)$$

where

$$\begin{aligned} & [(\delta E_{001})^2 + 3(\delta E_{111})^2]^{1/2} \\ &= 2[b^2(S_{11} - S_{12})^2 + \frac{1}{4}d^2S_{44}^2]^{1/2}X.\end{aligned}$$

For $\mathbf{X} \parallel [001]$ or $[111]$ (m_J is a good quantum number) the crystal is uniaxial and hence the expressions for the intensities [Eq. (7)] are independent of the azimuthal angle of the incident radiation about the stress axis. However this is not the case for $\mathbf{X} \parallel [110]$ since it has been shown above that m_J is no longer a good quantum number. For this stress direction the crystal is biaxial and the intensities of the various transitions will depend on the azimuthal angle of the incident radiation. In Appendix A we have derived expressions for the case of light incident along the [001] and [110] crystallographic directions. These results are listed below.

$$\begin{aligned}I_2^{11}(\mathbf{X}) &= I_2^{11}(0)[\eta/\Delta_0 - \gamma]^2, & I_2^{\perp}(\mathbf{X}) &= I_2^{\perp}(0)[\beta^2 \mp 2\beta\gamma/\sqrt{3} \pm 4\beta\eta/\sqrt{3}], \\ I_1^{11}(\mathbf{X}) &= I_1^{11}(0)[\beta^2 + \beta\Delta_0], & I_1^{\perp}(\mathbf{X}) &= I_1^{\perp}(0)[\beta^2 - 2\beta\alpha_0^{11} \mp 2\sqrt{3}\beta\gamma], \\ I_3^{11}(\mathbf{X}) &= I_3^{11}(0)[1 - 2\alpha_0^{11}], & I_3^{\perp}(\mathbf{X}) &= I_3^{\perp}(0)[1 + \alpha_0^{11} \mp 2\sqrt{3}\eta/\Delta_0],\end{aligned}\quad (14)$$

where the upper and lower sign refer to light incident along [001] and [110], respectively, and

$$\begin{aligned}\xi &= \frac{1}{8}(\delta E_{001} + 3\delta E_{111}), \\ \eta &= \frac{1}{8}\sqrt{3}(\delta E_{001} - \delta E_{111}), \\ \beta &= \eta / \{ \eta^2 + [\xi - (\xi^2 + \eta^2)^{1/2}]^2 \}^{1/2}, \\ \gamma &= \frac{(\xi^2 + \eta^2)^{1/2} - \xi}{\{ \eta^2 + [\xi - (\xi^2 + \eta^2)^{1/2}]^2 \}^{1/2}}, \\ \alpha_0^{11} &= \xi / \Delta_0.\end{aligned}\quad (15)$$

Because of the mixing of the $m_J = \pm \frac{3}{2}$ and $m_J = \pm \frac{1}{2}$ states, $I_2^{11} \neq 0$ contrary to the case of $\mathbf{X} \parallel [001]$ or $[111]$. The presence of this transition is a means of determining whether or not $\delta E_{001} = \delta E_{111}$.

Plotted in Fig. 9 are the energies of the $E_0(1)$, $E_0(2)$, and $E_0 + \Delta_0$ peaks of Ge as a function of [110] stress for light incident along [001] and [110]. Although the curves for the different directions of the incident light are displaced slightly, an effect which may be due to slightly different electric fields since the measurements were performed on two different samples, the slopes of the curves are the same within the experimental error. In Fig. 10 we have plotted the energies of the $E_0(1)$, $E_0(2)$, and $E_0 + \Delta_0$ peaks of GaAs as a function of stress for light incident along [001]. Measurements for this material were made for only one direction of the incident radiation since (1) no comparison can be made between the experimental values of the intensities and Eq. (14), for the reason mentioned in Sec. III A 1, and (2) the energy shifts of these peaks are independent of the direction of the incident radiation.

Listed in Table II are the values of $[b^2(S_{11} - S_{12})^2 + \frac{1}{4}d^2S_{44}^2]$ for Ge and GaAs as determined from Eq. (13) and the experimental data of Figs. 9 and 10, respectively. The measurement of this quantity for $\mathbf{X} \parallel [110]$ provides an internal check on the values of b and d . Table II shows that it is in good agreement

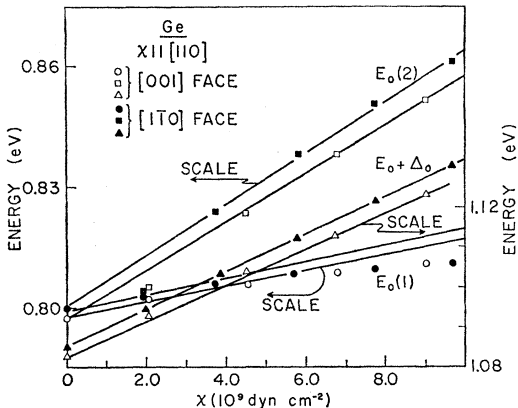


FIG. 9. Energies of the $E_0(1)$, $E_0(2)$, and $E_0 + \Delta_0$ peaks of Ge as a function of uniaxial stress along [110] observed for light incident on a [001] face and on a [110] face.

with the values deduced from the data for $\mathbf{X} \parallel [001]$ and $[111]$. Figures 11(a) and 11(b) show the electroreflectance spectra of the $E_0(1)$, $E_0(2)$, and $E_0 + \Delta_0$ peaks of Ge for light incident along [001] and [110], respectively, for the highest stress applied. In contrast to the case of $\mathbf{X} \parallel [001]$ or $[111]$, $E_0(2)$ appears for light polarized parallel to the stress axis. From Eq. (14) and the values of b and d listed in Table III the theoretical values of the intensity ratios I_1^{11}/I_1^1 , I_2^{11}/I_1^1 , and I_3^{11}/I_3^1 have been calculated for the case of light incident along [001] ($X = 9.02 \times 10^9$ dyn cm $^{-2}$) and [110] ($X = 9.68 \times 10^9$ dyn cm $^{-2}$). In Table III these values are compared with the experimental ones as determined from Figs. 11(a) and 11(b). The agreement for both cases is only qualitative.

B. Transitions in the [111] Direction: E_1 and $E_1 + \Delta_1$ Peaks

Band-structure calculations²⁷⁻³² have indicated that the E_1 and $E_1 + \Delta_1$ reflectance and electroreflectance

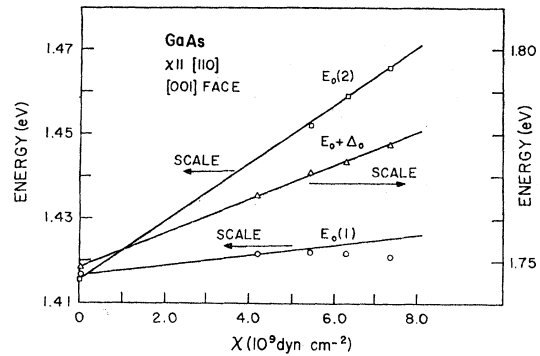


FIG. 10. Energies of the $E_0(1)$, $E_0(2)$, and $E_0 + \Delta_0$ peaks of GaAs as a function of uniaxial stress along [110] observed for light incident on a [001] face.

peaks of Ge and GaAs are caused by direct transitions at points in \mathbf{k} space along the eight equivalent [111] directions as shown in Fig. 12. Piezoreflectance experiments by Gerhardt² confirm this conclusion for germanium. Since uniaxial stress does not remove the inversion symmetry of the crystal, we need not consider all eight critical points but only those four in the [111], $[1\bar{1}\bar{1}]$, $[\bar{1}1\bar{1}]$, and $[\bar{1}\bar{1}1]$ directions. The application of a uniaxial stress along [001] should not remove the degeneracy of these bands (no interband splitting) but should produce an intraband splitting, i.e., a stress-

²⁷ B. Drust, Phys. Rev. **134**, A1337 (1964).

²⁸ M. Cardona and F. H. Pollak, Phys. Rev. **142**, 530 (1966).

²⁹ F. Herman, R. L. Kortum, C. D. Kuglin, and R. A. Short, in *Quantum Theory of Atoms, Molecules, and the Solid State*, edited by P. O. Löwdin (Academic Press Inc., New York, 1966) p. 381; also, J. Phys. Soc. Japan Suppl. **21**, 7 (1966).

³⁰ M. L. Cohen and T. K. Bergstresser, Phys. Rev. **141**, 789 (1966).

³¹ G. Dresselhaus, and M. S. Dresselhaus, Phys. Rev. **160**, 649 (1967).

³² F. H. Pollak, C. W. Higginbotham, and M. Cardona, J. Phys. Soc. Japan Suppl. **21**, 20 (1966).

splitting of the Λ_3 -orbital valence bands. Since the orbital bands are already split by the spin-orbit interaction, the effect of the orbital intraband stress splitting is to change the spin-orbit splitting. As will be shown later, this effect is quadratic in the ratio α of orbital intraband stress splitting to spin-orbit splitting. However, the stress-induced coupling of the orbital valence bands has a first-order effect on the wave functions of these bands and hence on the matrix elements for optical transitions, which can be observed as stress-induced

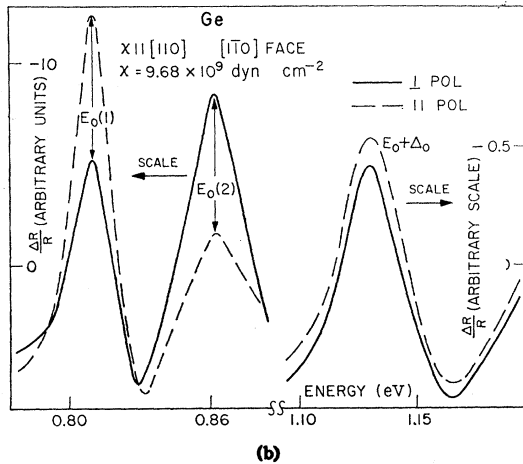
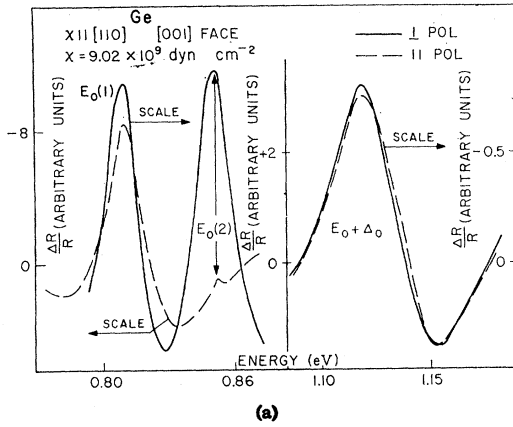


FIG. 11. Electrodiffractance peaks $E_0(1)$, $E_0(2)$, and $E_0 + \Delta_0$ of Ge for [110] stress with light incident along (a) [001] for a stress of 9.02×10^9 dyn cm^{-2} and (b) [110] for a stress of 9.68×10^9 dyn cm^{-2} .

polarization dependence of the intensities of the E_1 and $E_1 + \Delta_1$ peaks. In addition the hydrostatic pressure component of the strain will produce a shift in the center of gravity of the E_1 and $E_1 + \Delta_1$ peaks. The application of stress parallel to [111] will cause both an inter- and intraband splitting: The four levels will divide up into two groups of one and three levels, respectively. Since optical transitions between the Λ_3 valence and Λ_1 conduction bands are allowed only for the electric field of the incident light polarized perpendicular to the axis of the ellipsoid, for light polarized parallel to the stress

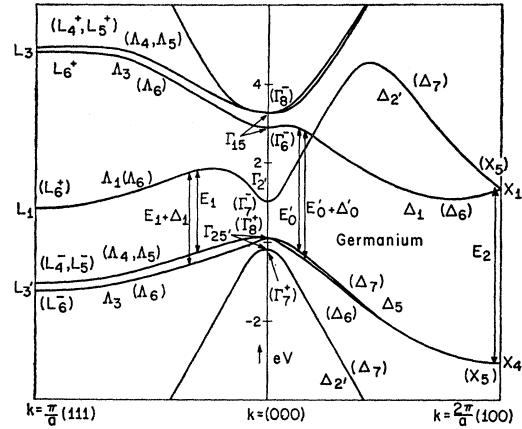


FIG. 12. Band structure of Ge obtained by the $\mathbf{k} \cdot \mathbf{p}$ method (see Refs. 28 and 32). The band structure of GaAs is qualitatively similar except for the removal of the degeneracy at X_1 .

axis only transitions between the second group of levels will occur, while for the case of light polarized perpendicular to the stress axis transitions between both groups will be observed. In addition to this interband splitting there will be an intraband effect for those bands whose \mathbf{k} vectors do not lie along the stress axis. As for the case of [001] stress this effect will be of second order in the energy eigenvalues but of first order in the optical transition matrix elements.

Most of the band-structure calculations²⁷⁻³² indicate the Λ_3 valence bands and the Λ_1 conduction band of Ge and GaAs are nearly parallel along the [111] direction. In Refs. 19, 22, 23, 27, 28, 30, 31, and 32 critical points are obtained only at about $(2\pi/a_i)[0.2, 0.2, 0.2]$, where a_i is the lattice constant, and at the edge of the BZ. The $(2\pi/a_i)[0.2, 0.2, 0.2]$ critical point is of the M_1 type and the one at the edge of the BZ is an M_0 type. Since the bands along Λ are nearly parallel, the nature and number of critical points can be changed by slight alterations³⁰ of the parameters of the band calculation. The line shape of the E_1 , $E_1 + \Delta_1$ electroreflectance peaks of GaAs indicate that they are caused by M_1 critical points.^{6,24} While the line shape of these peaks for Ge is not of M_1 type at room temperature, recent investigating³³ at 77°K by Seraphin's technique³ give peaks of the M_1 type. We shall, therefore, assume that the E_1 , $E_1 + \Delta_1$ peaks for both these materials are caused by the $(2\pi/a_i)[0.2, 0.2, 0.2]$ critical points.

The wavefunctions of the valence and conduction bands at this point have been obtained as a linear combinations of the $\mathbf{k} = 0$ wavefunctions from the $\mathbf{k} \cdot \mathbf{p}$ calculation.^{28,32} It is found that the Λ_3 valence bands at the critical point are composed mainly of contributions from $\Gamma_{25'}$ (Γ_{15}) while the Λ_1 conduction band consists of approximately 50% Γ_2' (Γ_1) and 50% Γ_{15} (Γ_{15}). These wavefunctions for Ge and GaAs at $(2\pi/a_i)[0.2, 0.2, 0.2]$ are listed in Appendix B. It can be easily shown that the

³³ K. L. Shaklee (private communication).

$\mathbf{k} \cdot \mathbf{p}$ term in the total Hamiltonian²⁸ does not contribute to changes with stress of the optical direct transitions. Once the linear combinations of $\mathbf{k}=0$ wavefunctions which compose a state of finite \mathbf{k} are known, the strain Hamiltonian of Eq. (1) can be used to describe the effects of the applied stress on these bands.

$$\left\| \begin{array}{c} |\bar{u}_{v1}\rangle \\ \frac{1}{2}\Delta_1 - [A^2a + B^2a'](S_{11} + 2S_{12})X \\ -\frac{1}{2}\delta E_{001} \end{array} \right\|$$

where A and B are defined in Appendix B, a' is the hydrostatic pressure deformation potential of the Γ_{15} (Γ_{15}) conduction bands relative to the $\Gamma_{25'}$ (Γ_{15}) valence bands, and Δ_1 is the spin-orbit splitting of the Λ_3 valence bands (0.21 eV for Ge and 0.23 eV for GaAs). The diagonalization of Eq. (16) yields, for the change in the energy separation between the conduction and valence bands,

$$\Delta(E_c - E_{v1}) = -\frac{1}{2}\Delta_1 + \delta E_H(\Lambda) - \frac{1}{2}[(\Delta_1)^2 + (\delta E_{001})^2]^{1/2},$$

$$\Delta(E_c - E_{v2}) = \frac{1}{2}\Delta_1 + \delta E_H(\Lambda) + \frac{1}{2}[(\Delta_1)^2 + (\delta E_{001})^2]^{1/2}, \quad (17)$$

where $\delta E_H(\Lambda) = [A^2a + B^2a'](S_{11} + 2S_{12})X$ is the mean shift of the energy bands due to the hydrostatic component of the strain. The first part of Eq. (17) refers to the E_1 peak, while the second corresponds to the $E_1 + \Delta_1$ peak.

In the notation of Brooks²⁴ the stress-induced shift of a critical point is given by

$$\Delta E = \mathbf{n} \cdot \{ \mathcal{E}_1(\epsilon_{xx} + \epsilon_{yy} + \epsilon_{zz})\mathbf{1} + \mathcal{E}_2[\boldsymbol{\epsilon} - \frac{1}{3}(\epsilon_{xx} + \epsilon_{yy} + \epsilon_{zz})\mathbf{1}] \} \cdot \mathbf{n}, \quad (18)$$

where \mathbf{n} is the unit vector in the direction of the critical point in \mathbf{k} space, $\mathbf{1}$ is the unit diadic, $\boldsymbol{\epsilon}$ is the strain tensor and \mathcal{E}_1 and \mathcal{E}_2 ³⁵ are the hydrostatic and shear-deformation potentials, respectively. For [001] stress Eq.

$$I_{E_1}^{II}(\mathbf{X}) = I_{E_1}^{II}(0)(1 + \alpha_1)$$

$$I_{E_1 + \Delta_1}^{II}(\mathbf{X}) = I_{E_1 + \Delta_1}^{II}(0)(1 - \alpha_1)$$

Shown in Figs. 13 and 14 are the electroreflectance spectra of the E_1 , $E_1 + \Delta_1$ peaks of Ge and GaAs, respectively, for zero stress and stress along [001] with the incident light polarized parallel and perpendicular to the stress axis. For the case of Ge the light is incident on a [110] face while for GaAs it strikes a [100] face. At zero stress there is a slight polarization dependence of the intensities, particularly for Ge, which may be due to the electric field at the semiconductor-electrolyte interface. The polarization dependence of the intensities as a function of stress is in agreement with Eqs. (21):

³⁴ H. Brooks, *Advances in Electronics and Electron Physics*, edited by L. Marton (Academic Press Inc., New York, 1955), Vol. 7, p. 85.

³⁵ We have used \mathcal{E} 's to indicate the deformation potentials in order to avoid confusion with the symbol used for energy.

1. Stress Parallel to [001]

From the strain and spin-orbit Hamiltonian of Eqs. (1a) and (1b) and the wavefunctions listed in Appendix B, the Hamiltonian for the energy difference between the Λ_1 conduction band and the Λ_3 valence bands is

$$\left\| \begin{array}{c} |\bar{u}_{v2}\rangle \\ -\frac{1}{2}\delta E_{001} \\ \frac{1}{2}\Delta_1 - [A^2a + B^2a'](S_{11} + 2S_{12})X \end{array} \right\|, \quad (16)$$

(18) yields only a hydrostatic shift for the [111] critical points which is given by

$$\Delta E = \mathcal{E}_1(S_{11} + 2S_{12})X = \delta E_H(\Lambda) \quad (19)$$

and hence from Eqs. (17) and (19) $\mathcal{E}_1 = (A^2a + B^2a')$.

For the case of $\delta E_{001} \ll \Delta_1$ Eq. (17) can be expanded in powers of $\delta E_{001}/\Delta_1$, giving

$$\Delta(E_c - E_{v1}) = -\frac{1}{2}\Delta_1 + \delta E_H(\Lambda) - \frac{1}{4}(\delta E_{001})^2/\Delta_1 + \dots$$

$$\Delta(E_c - E_{v2}) = +\frac{1}{2}\Delta_1 + \delta E_H(\Lambda) + \frac{1}{4}(\delta E_{001})^2/\Delta_1 + \dots \quad (20)$$

These expressions apply for all the Λ_3 - Λ_1 transitions and hence there is no interband splitting. However, the last term in Eq. (20) is produced by the orbital intraband splitting. Equation (20) indicates that uniaxial stress will cause a shift of the center of gravity of the E_1 and $E_1 + \Delta_1$ peaks and an increase in the energy separation between these two peaks. Although the intraband splitting is of second order in the ratio $\alpha_1 = \delta E_{001}/\Delta_1$ it is shown in Appendix B that the action of the stress produces first-order variations in the wave functions of the Λ_3 valence bands and therefore first order effects appear in the matrix elements for the optical transitions. From Appendix B, the stress-induced variations in the intensity of the E_1 , $E_1 + \Delta_1$ transitions for light polarized parallel and perpendicular to the stress axis, to first order in α_1 , is given by

$$I_{E_1}^I(\mathbf{X}) = I_{E_1}^I(0)(1 - \frac{1}{2}\alpha_1)$$

$$I_{E_1 + \Delta_1}^I(\mathbf{X}) = I_{E_1 + \Delta_1}^I(0)(1 + \frac{1}{2}\alpha_1). \quad (21)$$

$I^{II} > I^I$ for the E_1 peak while $I^{II} < I^I$ for the $E_1 + \Delta_1$ peak. In Figs. 15 and 16 we have plotted the various intensities as a function of stress for Ge and GaAs, respectively. For the case of Ge the intensities have been measured relative to the zero of scale while for GaAs the intensities have been measured relative to the minima preceding the peak, i.e., peak to peak. Since the line shape of the GaAs signal (Fig. 14) is in qualitative agreement with the theory of Aspnes²⁴ for an M_1 critical point it is appropriate to measure these intensities peak to peak. Because of the large lifetime broadening of the Ge spectrum (Fig. 13) there is considerable interference between the E_1 and $E_1 + \Delta_1$ structures. Since the lines shape does not agree with theory the reference for the peak heights is somewhat arbitrary.

We have found that the best agreement with theory for Ge is achieved if the intensities are taken relative to zero. The dashed lines in Figs. 15 and 16 represent the theoretical values of the intensities as calculated from Eqs. (21) using the values of b listed in Table II for Ge and GaAs, respectively, and the experimental values of the zero stress intensities, $I(0)$. For the case of GaAs the experimental and theoretical results are in very good agreement. The data for Ge, however, agrees only qualitatively with Eq. (21). However, we find that if the ratio I^{\parallel}/I^{\perp} for E_1 and $E_1+\Delta_1$ is plotted as a function of the applied stress the agreement with theory is quite

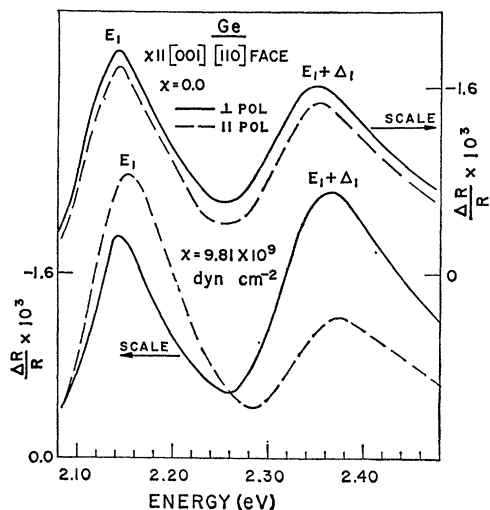


FIG. 13. E_1 and $E_1+\Delta_1$ electroreflectance peaks of Ge for zero stress and for a stress of 9.81×10^9 dyn cm^{-2} along $[001]$ with light polarized parallel and perpendicular to the stress axis.

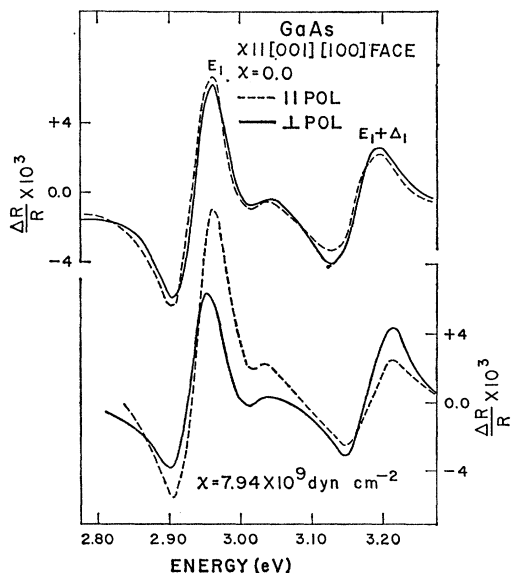


FIG. 14. E_1 and $E_1+\Delta_1$ electroreflectance peaks of GaAs for zero stress and for a stress of 7.94×10^9 dyn cm^{-2} along $[001]$ with light polarized parallel and perpendicular to the stress axis.

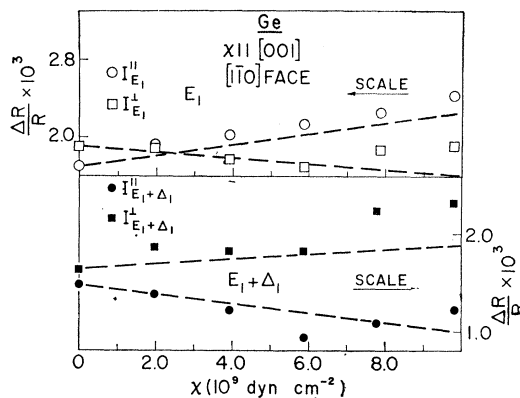


FIG. 15. The intensities of the E_1 and $E_1+\Delta_1$ electroreflectance peaks of Ge for light polarized parallel and perpendicular to the stress axis as a function of uniaxial stress along $[001]$.

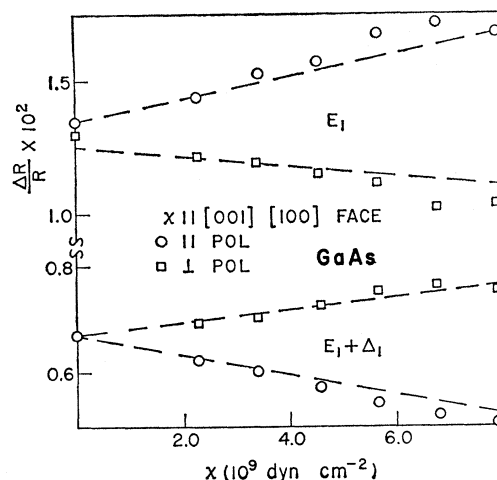


FIG. 16. The intensities of the E_1 and $E_1+\Delta_1$ electroreflectance peaks of GaAs for light polarized parallel and perpendicular to the stress axis as a function of uniaxial stress along $[001]$.

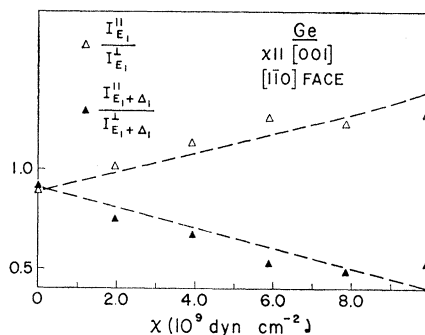


FIG. 17. The intensity ratio I^{\parallel}/I^{\perp} for the E_1 and $E_1+\Delta_1$ electroreflectance peaks of Ge as a function of $[001]$ stress.

good. The experimental and calculated values (dashed lines) for these ratios are shown in Fig. 17. Similar results can be seen qualitatively in the piezoreflectance data of Gerhardt² for Ge.

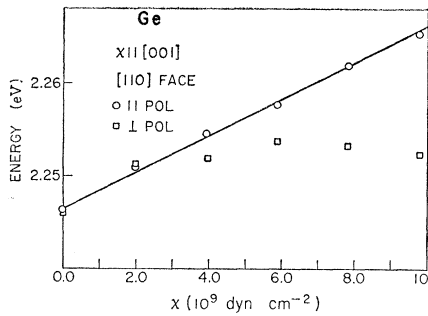


FIG. 18. The energy of the center of gravity of the E_1 and $E_1 + \Delta_1$ peaks of Ge, as a function of [001] stress, for light polarized parallel and perpendicular to the stress axis.

In Figs. 18 and 19 we have plotted the center of gravity of the E_1 and $E_1 + \Delta_1$ peaks as a function of stress for Ge and GaAs, respectively, for light polarized parallel and perpendicular to the stress axis. According to Eqs. (17) and (19) the center of gravity should have a linear stress dependence, the slope of the curve being $\mathcal{E}_1(S_{11} + 2S_{12})$. For the case of light polarized parallel to the stress axis the stress dependence of the center of gravity is linear for both Ge and GaAs. The values of \mathcal{E}_1 determined from this data for these materials is listed in Table II together with the values of \mathcal{E}_1 for Ge as determined by hydrostatic pressure and piezoreflectivity experiments. Our value of this parameter is somewhat lower than those deduced from the other measurements. The value of \mathcal{E}_1 for GaAs has not been determined previously. For light polarized perpendicular to the stress axis the curves are not linear but show a marked curvature at high stresses for both materials. We do not understand this behavior at present. Figures 20 and 21 show the difference in energy between the E_1 and $E_1 + \Delta_1$ peaks of Ge and GaAs, respectively, as a function of stress for light polarized parallel and perpendicular to the stress axis. For both materials this energy separation increases with increasing stress, thus producing an apparent increase in the spin-orbit splitting Δ_1 . Also plotted in these figures are the theoretical

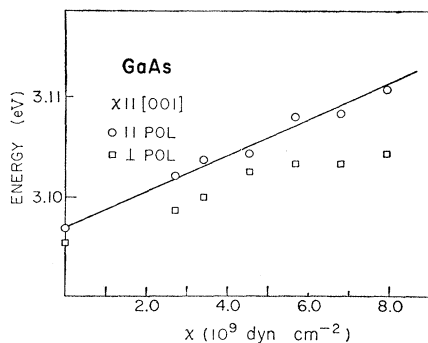


FIG. 19. The energy of the center of gravity of the E_1 and $E_1 + \Delta_1$ peaks of GaAs, as a function of [001] stress, for light polarized parallel and perpendicular to the stress axis.

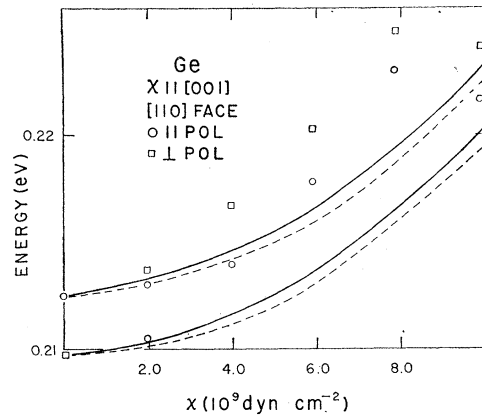


FIG. 20. The energy difference between the E_1 and $E_1 + \Delta_1$ peaks of Ge, as a function of [001] stress, for light polarized parallel and perpendicular to the stress axis. The dashed lines represent the theoretical value of this energy separation as determined from Eq. (20) while the solid lines show the combined effects of Eqs. (20) and (22).

values (dashed lines) of this energy separation as determined from Eq. (20) and the values of b listed in Table II. The experimental intraband splitting is considerably larger than that deduced from the theoretical expressions of Eq. (20). We have also considered the effect of the dilation on the spin-orbit interaction. According to a recent calculation by Brust and Liu³⁶ the fractional change of the spin-orbit splitting with lattice constant is given by

$$\delta(\Delta_1)/\Delta_1 \approx -4\delta(a_i)/a_i, \quad (22)$$

where a_i is the lattice constant. The combined effect of Eqs. (20) and (22) is also shown in Figs. 20 and 21 (solid lines). This combined effect does not fully explain the observed increase in the energy separation of the $E_1 + \Delta_1$, E_1 peaks.

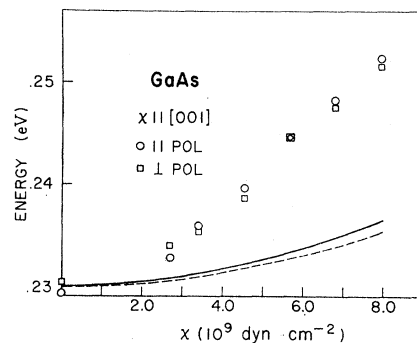


FIG. 21. The energy difference between the E_1 and $E_1 + \Delta_1$ peaks of GaAs, as a function of [001] stress, for light polarized parallel and perpendicular to the stress axis. The dashed lines represent the theoretical value of this energy separation as determined from Eq. (20) while the solid lines show the combined effects of Eqs. (20) and (22).

³⁶ D. Brust and L. Liu, Solid State Commun. 4, 193 (1966).

2. Stress Parallel to [111]

a. *Bands along [111]*. From the wavefunctions listed in Appendix B and Eqs. (1a) and (1b), the Hamiltonian for the energy difference between the conduction- and valence-band points whose \mathbf{k} vector lies along the direction of the stress is given by

$$\begin{vmatrix} \langle \bar{u}_{v1} | & \langle \bar{u}_{v2} | \\ \frac{1}{2}\Delta_1 - \delta E_H(\Lambda) & 0 \\ + B^2 \delta E_{111}' + \frac{1}{2} \delta E_{111} & \\ 0 & -\frac{1}{2}\Delta_1 - \delta E_H(\Lambda) \\ + B^2 \delta E_{111}' + \frac{1}{2} \delta E_{111} & \end{vmatrix}, \quad (23)$$

where $\delta E_{111}' = (d'/\sqrt{3})S_{44}X$ is the splitting of the Γ_{15} (Γ_{15}) conduction bands and d' is the shear-deformation potential of these bands for strains of rhombohedral symmetry.

The diagonalization of Eq. (23) yields

$$\begin{aligned} \Delta(E_c - E_{v1}) &= -\frac{1}{2}\Delta_1 + \delta E_H(\Lambda) - B^2 \delta E_{111}' - \frac{1}{2} \delta E_{111}, \\ \Delta(E_c - E_{v2}) &= +\frac{1}{2}\Delta_1 + \delta E_H(\Lambda) - B^2 \delta E_{111}' - \frac{1}{2} \delta E_{111}. \end{aligned} \quad (24)$$

For stress parallel to [111], Eq. (18) gives, for the stress-induced energy changes of critical points along this direction,

$$\Delta E = \mathcal{E}_1(S_{11} + 2S_{12})X + \frac{1}{3}\mathcal{E}_2 S_{44}X. \quad (25)$$

Hence, from Eqs. (24) and (25), $\mathcal{E}_2 = -\sqrt{3}(B^2 d' + \frac{1}{2}d)$.

The intensities for the various polarization, as calculated from the wavefunctions in Appendix B, are given

$$\begin{aligned} I_{E_1}^{||}(X) &= I_{E_1}^{||}(0)(1 + \frac{4}{3}\alpha_1'), \\ I_{E_1+\Delta_1}^{||}(X) &= I_{E_1+\Delta_1}^{||}(0)(1 - \frac{4}{3}\alpha_1'), \end{aligned}$$

where $\alpha_1' = \delta E_{111}/\Delta_1$.

Equations (24) and (28) indicate that there should be an interband splitting between the bands in the [111] and $[\bar{1}\bar{1}\bar{1}]$, $[\bar{1}\bar{1}\bar{1}]$, and $[\bar{1}\bar{1}\bar{1}]$ directions which can be observed as a stress-induced splitting of E_1 , $E_1 + \Delta_1$ for light polarized perpendicular to the stress axis. Equations (26) and (29) show that for light polarized parallel to the stress axis only transitions between the latter group of bands will be observed. For these bands there should be an intraband splitting and associated variation of the intensities with stress.

Figures 22 and 23 show the electroreflectance spectra of the E_1 , $E_1 + \Delta_1$ peaks of Ge and GaAs, respectively, with stress parallel to [111] with light polarized parallel and perpendicular to the strain axis. For the latter polarization the splitting of the E_1 peak is clearly evident in both materials. There is some indication of splitting for the $E_1 + \Delta_1$ structure of GaAs, while for Ge only a broadening of this peak is seen. It is somewhat more difficult to observe energy splittings of this higher energy peak because of the smaller wavelength

by

$$\begin{aligned} I_{E_1}^{\perp}(X) &= 0, & I_{E_1}^{\perp}(X) &= I_{E_1}^{\perp}(0), \\ I_{E_1+\Delta_1}^{\perp}(X) &= 0, & I_{E_1+\Delta_1}^{\perp}(X) &= I_{E_1+\Delta_1}^{\perp}(0). \end{aligned} \quad (26)$$

As indicated in Eq. (26), transitions between bands along [111] are observed only for perpendicularly polarized light and since there is no intraband splitting for these bands there is no strain dependence of the intensities.

b. *Bands along $[\bar{1}\bar{1}\bar{1}]$, $[\bar{1}\bar{1}\bar{1}]$, and $[\bar{1}\bar{1}\bar{1}]$* . For stress parallel to [111] the bands in these three directions remain equivalent since their \mathbf{k} vectors have equal projections on the stress axis. The Hamiltonian for the energy difference between these conduction and valence bands is given by

$$\begin{vmatrix} \langle \bar{u}_{v1}' | & \langle \bar{u}_{v2}' | \\ \frac{1}{2}\Delta_1 - \delta E_H(\Lambda) & \frac{2}{3}\delta E_{111} \\ -\frac{1}{3}B^2 \delta E_{111}' - \frac{1}{6}\delta E_{111} & \\ \frac{2}{3}\delta E_{111} & -\frac{1}{2}\Delta_1 - \delta E_H(\Lambda) \\ -\frac{1}{3}B^2 \delta E_{111}' - \frac{1}{6}\delta E_{111} & \end{vmatrix}. \quad (27)$$

From the diagonalization of Eq. (27) and expansion in powers of $\delta E_{111}/\Delta_1$ we obtain

$$\begin{aligned} \Delta(E_c - E_{v1}) &= -\frac{1}{2}\Delta_1 + \delta E_H(\Lambda) + \frac{1}{3}B^2 \delta E_{111}' + \frac{1}{6}\delta E_{111} \\ &\quad - (4/9)(\delta E_{111})^2/\Delta_1 + \dots, \\ \Delta(E_c - E_{v2}) &= +\frac{1}{2}\Delta_1 + \delta E_H(\Lambda) + \frac{1}{3}B^2 \delta E_{111}' + \frac{1}{6}\delta E_{111} \\ &\quad + (4/9)(\delta E_{111})^2/\Delta_1 + \dots. \end{aligned} \quad (28)$$

From Eq. (27) and the wavefunctions in Appendix B the various intensities have been calculated to be

$$\begin{aligned} I_{E_1}^{\perp}(X) &= I_{E_1}^{\perp}(0)(1 - \frac{4}{3}\alpha_1'), \\ I_{E_1+\Delta_1}^{\perp}(X) &= I_{E_1+\Delta_1}^{\perp}(0)(1 + \frac{4}{3}\alpha_1'), \end{aligned} \quad (29)$$

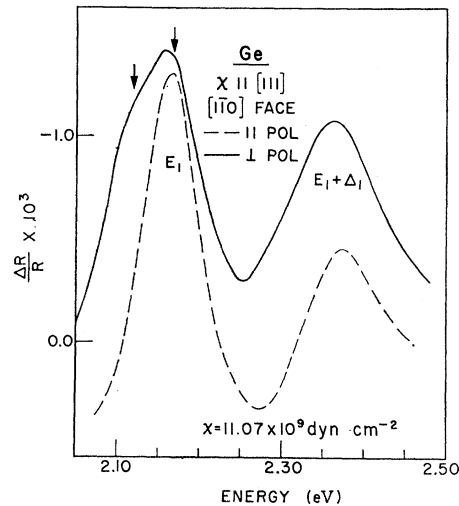


FIG. 22. Electroreflectance spectra of the E_1 and $E_1 + \Delta_1$ peaks of Ge for $X = 11.07 \times 10^9$ dyn cm^{-2} along [111] with light polarized parallel and perpendicular to the stress axis.

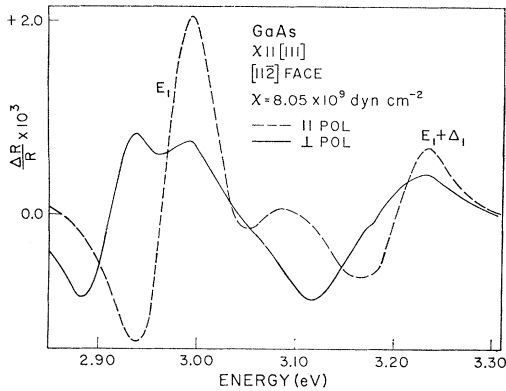


FIG. 23. Electroreflectance spectra of the E_1 and $E_1 + \Delta_1$ peaks of GaAs for $X = 8.05 \times 10^9 \text{ dyn cm}^{-2}$ along $[111]$ with light polarized parallel and perpendicular to the stress axis.

shift and larger lifetime broadening. From Eqs. (24), (25), and (27) and the experimentally observed splittings and shifts of the E_1 peak (see Fig. 23) we have determined the hydrostatic (\mathcal{E}_1) and shear (\mathcal{E}_2) deformation potentials of the Δ_1 - Δ_3 transitions of GaAs. These values are listed in Table II. For this material there is good agreement between the values of \mathcal{E}_1 as deduced from the experimental results for $[001]$ and $[111]$ stress. There has been no prior determinations of \mathcal{E}_2 for GaAs. For Ge we have encountered some difficulty in obtaining consistent values for \mathcal{E}_1 and \mathcal{E}_2 . We have indicated by arrows in Fig. 22 what seems to be a reasonable choice for the positions of the interband split E_1 peak. From Eqs. (24), (25), and (27) and the experimentally observed splitting and shift of this peak one obtains $\mathcal{E}_1 = -3.7 \pm 10\%$ eV and $\mathcal{E}_2 = +6.3 \pm 10\%$ eV. This \mathcal{E}_1 is smaller than that obtained from measurements for $[001]$ stress (see Table II) while the value of \mathcal{E}_2 is somewhat larger than that obtained by Gerhardt. The data of Fig. 22 can also be treated without the use of the somewhat poorly defined low-energy shoulder of E_1 for perpendicular polarization if we use the value of \mathcal{E}_1 obtained from $[001]$ stress measurements. In Fig. 24 we have plotted the energies of the E_1 and $E_1 + \Delta_1$

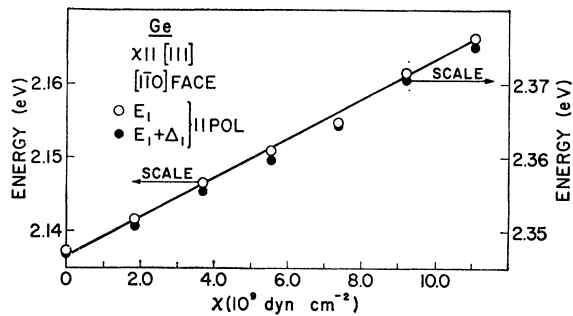


FIG. 24. The energies of the E_1 and $E_1 + \Delta_1$ peaks of Ge as a function of $[111]$ stress for light polarized parallel to the stress direction.

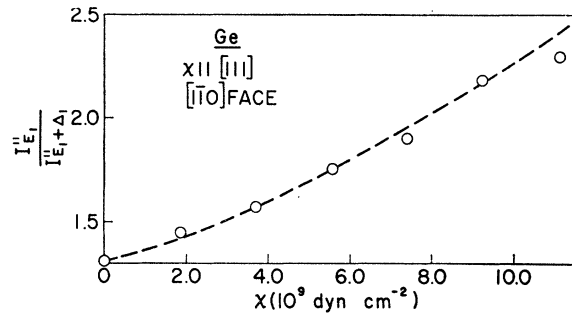


FIG. 25. The intensity ratio $I_{E_1}^{\parallel}/I_{E_1 + \Delta_1}^{\parallel}$ of Ge as a function of $[111]$ stress. The dashed line is the theoretical value of this ratio as determined from Eq. (29) and the value of d listed in Table II.

peaks of Ge for parallel polarization as a function of stress. We then find from the shift of the E_1 , $E_1 + \Delta_1$ peaks for parallel polarization and Eqs. (24) and (25) $\mathcal{E}_2 = +5.1 \pm 20\%$ eV, in good agreement with Gerhardt.

Figure 24 also indicates that there is no apparent increase in Δ_1 of the sort expected for intraband splitting for parallel polarization. [see Eq. (28)]. This is somewhat surprising in view of the fact that the intraband splitting for $[001]$ stress is larger than expected.

In Fig. 25 we have plotted the experimentally observed intensity ratio $I_{E_1}^{\parallel}/I_{E_1 + \Delta_1}^{\parallel}$ as a function of stress for Ge together with the theoretical values (dashed lines) as calculated from Eq. (29) and the value of d listed in Table II. As can be seen in the figure, the agreement is quite good. The stress-induced variations of I^{\parallel} are not subject to simple analysis because of the line shape changes produced by the interband splitting. Plotted in Fig. 26 are $I_{E_1}^{\parallel}$ and $I_{E_1 + \Delta_1}^{\parallel}$ for GaAs as a function of stress together with the theoretical values (dashed lines) for these intensities. The experimental values of $I_{E_1 + \Delta_1}^{\parallel}$ agree quite well with theory while there is a serious divergence for $I_{E_1}^{\parallel}$, a discrepancy which we do not understand at present.

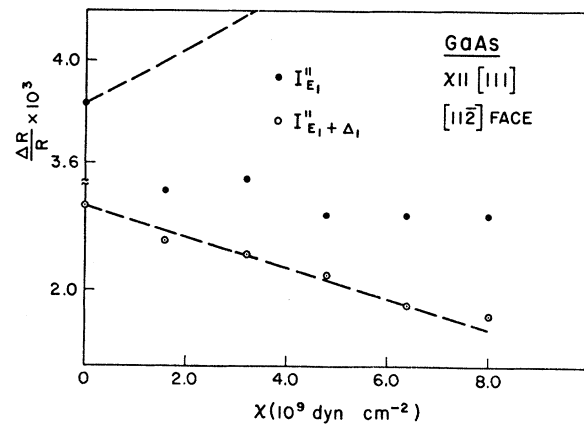


FIG. 26. The intensities $I_{E_1}^{\parallel}$ and $I_{E_1 + \Delta_1}^{\parallel}$ for GaAs as a function of $[111]$ stress. The dashed lines are the theoretical values as determined from Eq. (29) and the value of d listed in Table II.

3. Stress Parallel to [110]

From the spin-orbit and strain Hamiltonian of Eqs. (1a) and (11), and the wavefunctions listed in Appendix B, the energy difference between the conduction and valence bands has been calculated to be

$$\left\| \begin{array}{cc} \frac{1}{2}\Delta_1 - \delta E_H(\Lambda) & \pm \frac{1}{4}(2\delta E_{111} - \delta E_{001}) \\ \pm \frac{1}{2}B^2\delta E_{111}' \pm \frac{1}{4}\delta E_{111} & -\frac{1}{2}\Delta_1 - \delta E_H(\Lambda) \\ \pm \frac{1}{4}(2\delta E_{111} - \delta E_{001}) & \pm \frac{1}{2}B^2\delta E_{111}' \pm \frac{1}{4}\delta E_{111} \end{array} \right\|. \quad (30)$$

From the diagonalization of Eq. (30) and expansion in powers of $(2\delta E_{111} - \delta E_{001})/\Delta_1$ we obtain

$$\begin{aligned} \Delta(E_c - E_{v1}) &= -\frac{1}{2}\Delta_1 + \delta E_H(\Lambda) \mp \frac{1}{2}B^2\delta E_{111}' \mp \frac{1}{4}\delta E_{111} \\ &\quad - (2\delta E_{111} - \delta E_{001})^2/16\Delta_1, \\ \Delta(E_c - E_{v2}) &= +\frac{1}{2}\Delta_1 + \delta E_H(\Lambda) \mp \frac{1}{2}B^2\delta E_{111}' \mp \frac{1}{4}\delta E_{111} \\ &\quad + (2\delta E_{111} - \delta E_{001})^2/16\Delta_1, \end{aligned} \quad (31)$$

where the upper sign refers to the bands along [111] and $[\bar{1}\bar{1}\bar{1}]$ while the lower sign refers to the bands along $[\bar{1}\bar{1}\bar{1}]$ and $[\bar{1}\bar{1}\bar{1}]$.

The stress-dependent intensity for light polarized parallel to the stress axis for either face have been determined to be

$$\begin{aligned} I_{E_1''}(X) &= I_{E_1''}(0)[1 - \frac{1}{2}\alpha_1''], \\ I_{E_1+\Delta_1''}(X) &= I_{E_1+\Delta_1''}(0)[1 + \frac{1}{2}\alpha_1''] \end{aligned} \quad (32)$$

for both sets of bands, where $\alpha_1'' = (2\delta E_{111} - \delta E_{001})/\Delta_1$.

For the case of perpendicular polarization the intensities for light incident on a [001] face are given by

$$\begin{aligned} I_{E_1^\perp}(X) &= I_{E_1^\perp}(0)[1 \pm \frac{1}{2}\alpha_1'^\perp], \\ I_{E_1+\Delta_1^\perp}(X) &= I_{E_1+\Delta_1^\perp}(0)[1 \pm \frac{1}{2}\alpha_1'^\perp], \end{aligned} \quad (33)$$

where the upper sign refers to the [111] and $[\bar{1}\bar{1}\bar{1}]$ transitions and the lower sign to the other set. For a $[\bar{1}\bar{1}\bar{0}]$ face the intensities have the same form as Eq. (33) except that the signs are interchanged.

For this stress direction transitions between both sets of bands are allowed for both polarization directions and hence clear-cut polarization-dependent effects, such as intensity variations and splittings, are difficult to detect. However, the observed stress-dependent intensities and energy shifts are in qualitative agreement with Eqs. (31)–(33).

C. E_0' Peaks of Silicon

The origin of the structure in the reflectivity and electroreflectance spectra of Si at about 3.4 eV (E_0') has been the source of considerable controversy. According to one viewpoint this peak (or peaks in the case of electroreflectance) is caused by $\Delta_5-\Delta_1$ transitions (along [100] axes) in the vicinity of the Γ point. The main experimental arguments given for this assignment are the chemical-shift data of Tauc and Abraham on Ge-Si alloys,³⁷ dc² and ac³⁸ piezoreflectivity, and certain elec-

troreflectance experiments.³⁹ Gerhardt² found that dc uniaxial stress along [111] shifts the 3.4-eV reflectivity peak equally for light polarized parallel and perpendicular to the stress direction, while [001] stress splits the peak into two polarization-dependent components. This behavior strongly suggest Δ symmetry although it is not conclusive.²⁹ Theoretical band calculations by the pseudopotential method²⁷ also associate the E_0' peak with [100] transitions near Γ .

However, some doubts regarding the Δ assignment have been raised by the theoretical calculations of Goroff and Kleinman,¹ Kane,⁴⁰ and Herman *et al.*²⁹ Goroff and Kleinman's pseudopotential calculations of the deformation potentials of Si yields a value for the pressure coefficient of the Δ transition which is in serious disagreement with the experimental value. They suggested that E_0' might be due to the $L_3'-L_1$ (or $\Lambda_3-\Lambda_1$) transitions, for which the agreement was considerably better. Herman *et al.* have challenged the Δ assignment on the basis of their theoretical estimate of (1) the $\Gamma_{25'}-\Gamma_{15}$ gap of 2.8 eV rather than 3.4 eV and (2) the pressure coefficient along Δ , which is considerably smaller than the experimental value. The calculations of both Herman *et al.* and Kane indicate that an extended region of the BZ is responsible for this structure including regions near the Λ axes.

With the greater resolution and sensitivity of the electroreflectance technique, as opposed to reflectivity, we felt that new information concerning the E_0' structure might be obtained from a piezo-electroreflectance experiment. We have investigated the stress dependence of this structure for stress along [001], [111], and [110] with light incident on several different faces.

1. Stress Parallel to [001]

In Figs. 27(a)–27(d) are plotted the electroreflectance spectra of the E_0' peaks of Si for $X=0.0$, 3.47×10^9 dyn cm⁻², 9.02×10^9 dyn cm⁻², and 14.22×10^9 dyn cm⁻² along [001] with light incident on a [110] face and polarized parallel and perpendicular to the stress axis. For this material there are significant polarization effects at zero stress for light incident on this face.⁶ Figure 27(a) shows that for perpendicular polarization there are two distinct peaks, which are labeled $E_0'(1)$ and $E_0'(2)$. For parallel polarization only one peak $E_0'(4)$, appears clearly, while there is only a small shoulder $E_0'(3)$ at approximately the energy of $E_0'(1)$. This polarization effect is probably due to the large "inherent" surface electric field along the low-symmetry direction [110]. Figure 27(b) indicates that the application of [001] stress causes: (a) $E_0'(1)$ and $E_0'(2)$ to move apart in energy, thus becoming more clearly re-

³⁷ J. Tauc and A. Abraham, in *Proceedings of the International Conference on Semiconductor Physics, Prague, 1960* (Czechoslovakian Academy of Sciences, Prague, 1961), p. 375; also, J. Phys. Chem. Solids **20**, 190 (1961).

³⁸ G. O. Gobeli and E. O. Kane, Phys. Rev. Letters **15**, 142 (1965).

³⁹ B. O. Seraphin, Bull. Am. Phys. Soc. **11**, 272 (1966).

⁴⁰ E. O. Kane, Phys. Rev. **146**, 558 (1966).

³⁷ J. Tauc and A. Abraham, in *Proceedings of the International Conference on Semiconductor Physics, Prague, 1960* (Czechoslovakian Academy of Sciences, Prague, 1961), p. 375; also, J. Phys. Chem. Solids **20**, 190 (1961).

solved; (b) $E_0'(4)$ to move to slightly lower energies; and (c) $E_0'(3)$ to disappear. At higher stresses [Fig. 27(c)] $E_0'(2)$ splits, the two components being labeled $E_0'(2a)$ and $E_0'(2b)$, while $E_0'(1)$ and $E_0'(4)$ have moved to slightly lower energies. For the highest stress applied [Fig. 27(d)] $E_0'(2a)$ has almost merged with $E_0'(1)$ and a splitting of $E_0'(4)$ is clearly evident, these peaks are labeled $E_0'(4a)$ and $E_0'(4b)$.

Plotted in Figs. 28(a)–28(c) are the electroreflectance spectra of the E_0' peaks with light incident on a $[100]$ face for $X=0.0$, 10.12×10^9 dyn cm^{-2} and 15.57×10^9 dyn cm^{-2} . Figure 28(a) shows that there is only a slight polarization dependence, which may be due to the fact that the incident radiation makes a small angle ($\approx 10^\circ$) with the normal to the face. However, Figs. 28(b) and 28(c) show that the effects of the stress are the same as in the case of light incident on a $[110]$ face.

2. Stress parallel to $[111]$

The effect of $[111]$ stress on the E_0' peaks for light incident on a $[11\bar{2}]$ face is shown in Figs. 29(a)–29(c) for $X=0.0$, 7.11×10^9 dyn cm^{-2} , and 11.91×10^9 dyn cm^{-2} . Figures 30(a) and 30(b) show the spectra for $X=0.0$ and 9.48×10^9 dyn cm^{-2} with light incident on a $[1\bar{1}0]$ face.

For the case of light incident on a $[11\bar{2}]$ face there is some polarization dependence at zero stress [see Fig. 29(a)] although all four peaks, $E_0'(1)$, $E_0'(2)$, $E_0'(3)$, and $E_0'(4)$, are clearly evident. Peaks $E_0'(2)$ and $E_0'(4)$ appear at the same energy while $E_0'(1)$ is about 0.01 eV higher than $E_0'(3)$. Figure 30(a) shows that there are almost no polarization effects at zero stress (as required by symmetry) for the case of the $[1\bar{1}0]$ face. The application of stress along this direction causes (a) $E_0'(2)$ and $E_0'(3)$ to disappear and (b) very small energy

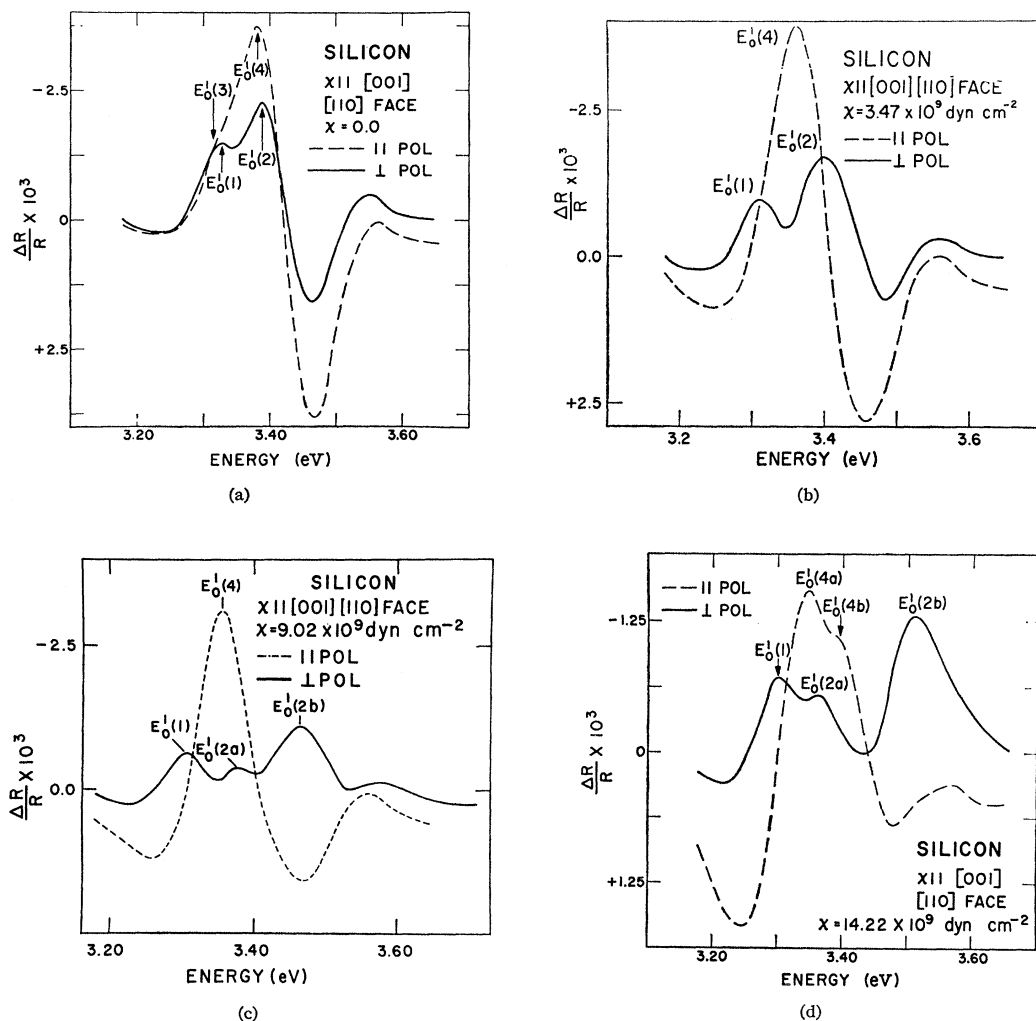
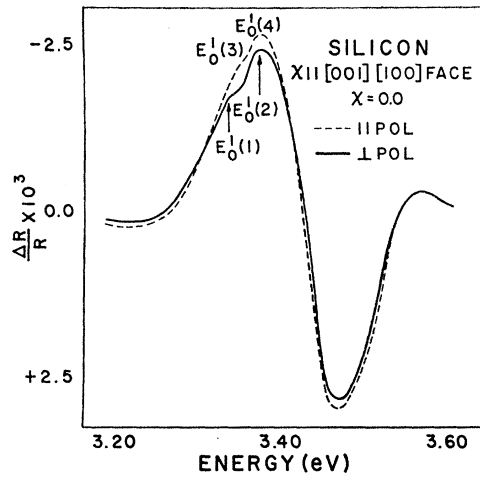
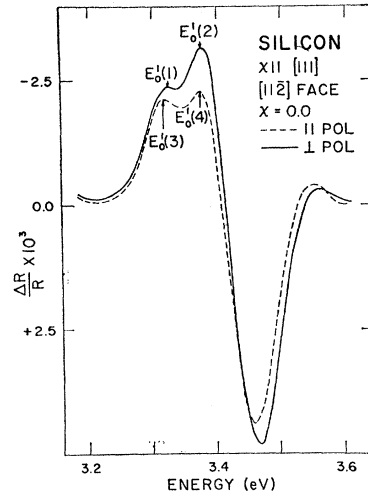


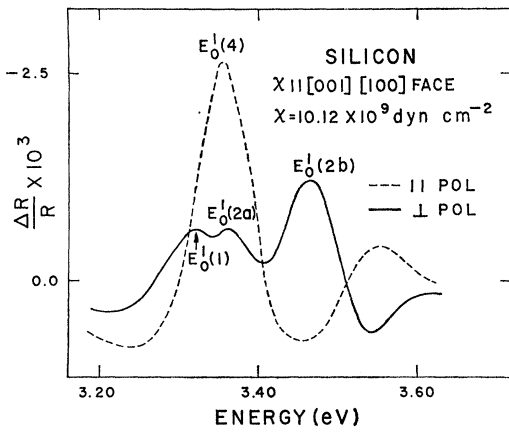
FIG. 27. The electroreflectance spectra of the E_0' peaks of Si for stress along $[001]$ with light incident on a $[110]$ face and polarized parallel and perpendicular to the stress axis for stresses of (a) 0.0, (b) 3.49×10^9 dyn cm^{-2} , (c) 9.02×10^9 dyn cm^{-2} , and (d) 14.22×10^9 dyn cm^{-2} .



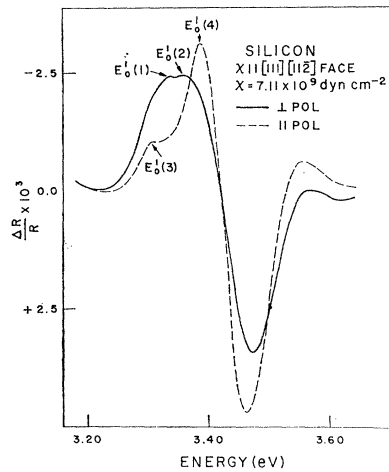
(a)



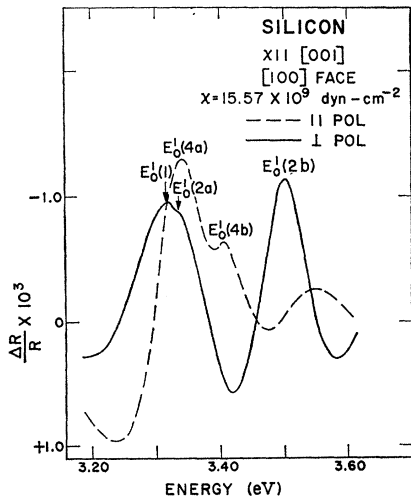
(a)



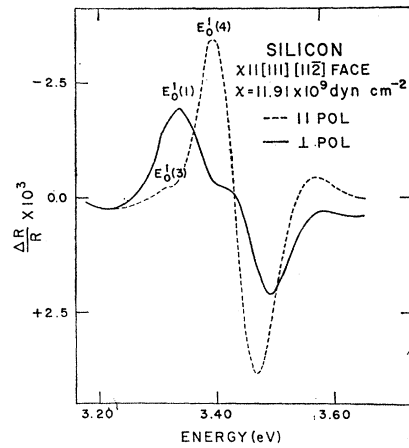
(b)



(b)



(c)



(c)

FIG. 28. The electroreflectance spectra of Si in the energy range 3.2–3.6 eV for [001] stress with light incident on a [100] face and polarized parallel and perpendicular to the stress axis for stresses of (a) 0.0, (b) 10.12×10^9 dyn cm^{-2} , and (c) 15.57×10^9 dyn cm^{-2} .

FIG. 29. The effect of [111] stress on the E_0' electroreflectance peaks of Si with light incident on a [112] face and polarized parallel and perpendicular to the stress axis for stresses of (a) 0.0, (b) 7.11×10^9 dyn cm^{-2} , and (c) 11.91×10^9 dyn cm^{-2} .

changes for $E_0'(1)$ and $E_0'(2)$ [see Figs. 29(b), 29(c), and 30(b)]. There are no splittings such as those observed for [001] stress.

3. Stress parallel to [110]

The effects of stress along [110] with light incident on a [001] face are shown in Figs. 31(a) ($X=0.0$) and 31(b) ($X=10.80 \times 10^9 \text{ dyn cm}^{-2}$). At zero-stress peaks $E_0'(2)$ and $E_0'(4)$ are clearly evident while there is only a slight indication of $E_0'(1)$ for perpendicular polarization. Application of the stress causes $E_0'(2)$ to split into two components labeled $E_0'(2a)$ and $E_0'(2b)$ in Fig.

31(b), the former peak moving to lower energies while the latter structure moves to higher energies. There is no evidence for $E_0'(1)$ at high stresses. The energy of $E_0'(4)$ has remained almost unchanged.

Shown in Fig. 32(a) is the spectrum of a sample with light incident on a [110] face at zero stress with light polarized parallel and perpendicular to the [110] axis. This figure and Fig. 27(a) are very similar except for

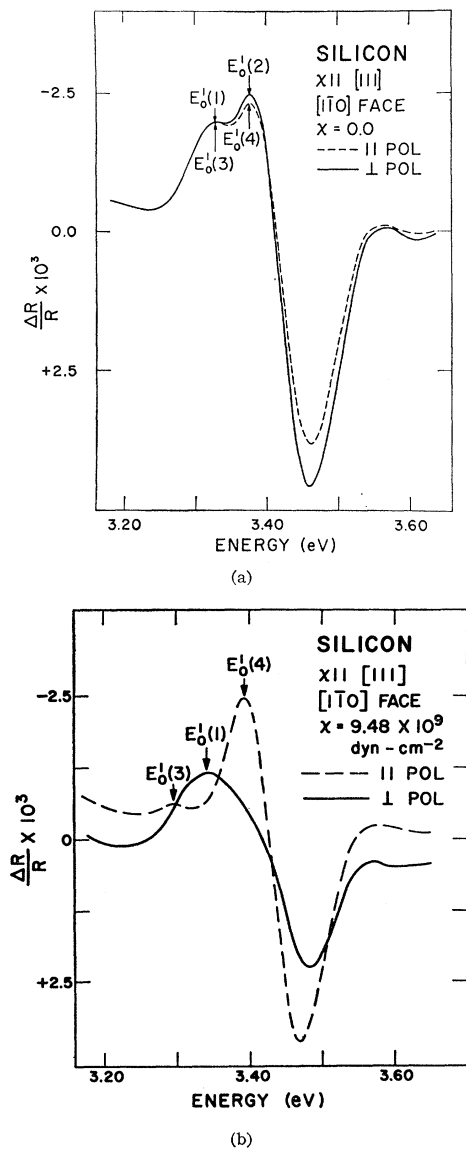


FIG. 30. The effect of [111] stress on the E_0' electroreflectance peaks of Si with light incident on a [110] face and polarized parallel and perpendicular to the stress axis for stresses of (a) 0.0 and (b) $9.48 \times 10^9 \text{ dyn cm}^{-2}$.

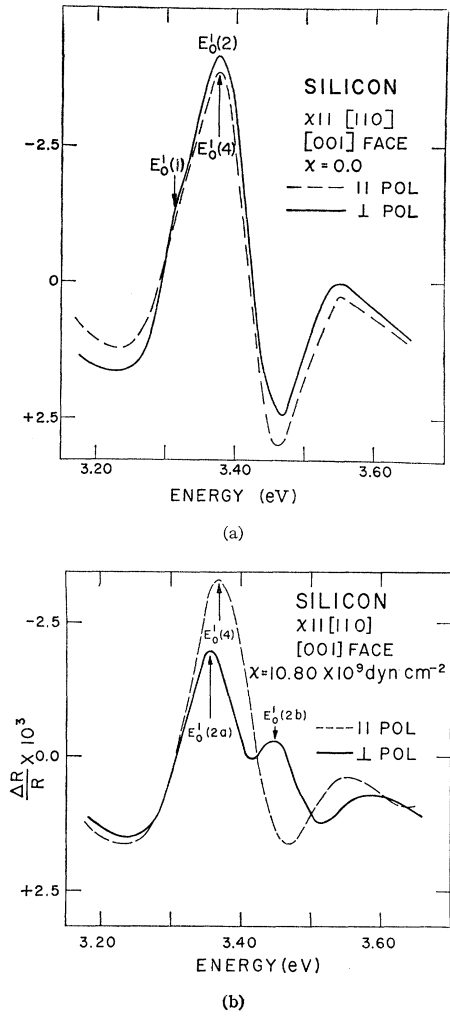


FIG. 31. The E_0' electroreflectance peaks of Si for stress along [110] with light incident on a [001] face and polarized parallel and perpendicular to the stress axis for stresses of (a) 0.0 and (b) $10.80 \times 10^9 \text{ dyn cm}^{-2}$.

the fact that the effects of the two polarizations have been interchanged. In Fig. 32(b) we have plotted the spectrum for $X=10.96 \times 10^9 \text{ dyn cm}^{-2}$. The energy of $E_0'(2)$ has increased by about 0.02 eV. $E_0'(1)$ has become more pronounced and seems to have shifted to lower energies by about 0.02 eV, although this is somewhat hard to determine since it appears as only a shoulder at zero stress. The energies of $E_0'(3)$ and $E_0'(4)$

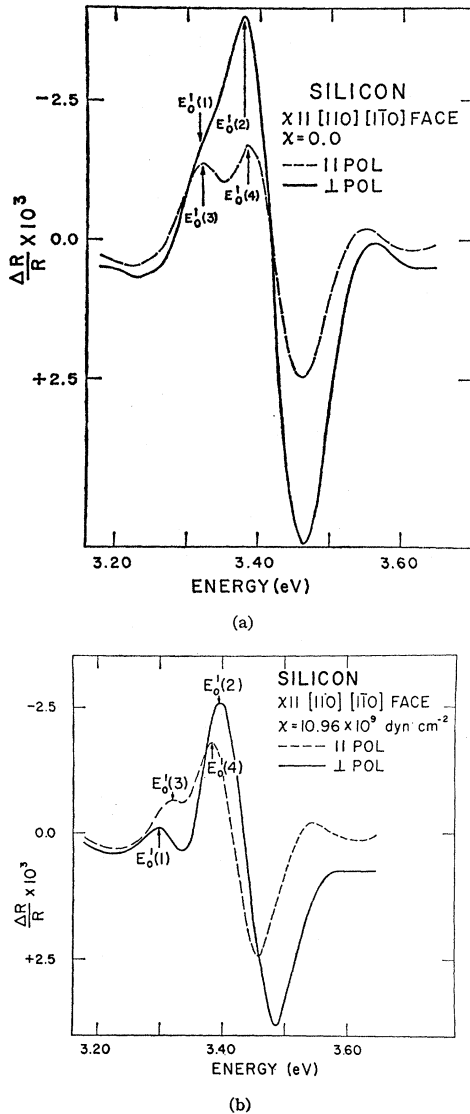


FIG. 32. Electroreflectance spectrum of Si in the energy range 3.2–3.6 eV for [110] stress with light incident on a $[1\bar{1}0]$ face and polarized parallel and perpendicular to the stress axis for stresses of (a) 0.0 and (b) 10.96×10^9 dyn cm⁻².

have not shifted although there has been a change in their relative intensities. In contrast to Fig. 31(b) there is no splitting of any of the peaks for light incident on a $[1\bar{1}0]$ face.

4. Discussion

The gross features of the piezo-electroreflectance spectra for the E'_0 peaks, i.e., splittings for [001] and [110] stresses and absence of such splittings for [111] stress, seem to indicate Δ_5 - Δ_1 interband transitions although there are a number of features which we have not been able to explain on this basis, even taking into account the intraband splitting of the Δ_5 valence band. A detailed analysis of Δ transitions near Γ similar to that per-

formed for the E_1 , $E_1 + \Delta_1$ peaks of Ge and GaAs is difficult since the Δ_2 valence band states (see Fig. 12) are strongly mixed into Δ_5 by this spin-orbit interaction. This interaction is usually neglected in considerations of the interband transitions in Si since spin-orbit splittings in this material are small ($\Delta_0 = 0.044$ eV, $\Delta'_0 \approx 0.025$ eV) compared with direct gaps. A complete analysis of the stress dependence of the density of states in the vicinity of the $\Gamma_{25'} - \Gamma_{15}$ transition is presently being carried out using the $\mathbf{k} \cdot \mathbf{p}$ scheme.³² However, as has been shown in Secs. III A and III B, intraband splittings and the associated intensity variations are a function of α , the ratio of orbital intraband stress splitting and the spin-orbit splitting. Since in Si this ratio will be on the order of unity for the highest stresses applied in this experiment, spin-orbit effects must be taken into consideration.

For [001] stress the behavior of peaks $E'_0(2a)$, $E'_0(2b)$, and $E'_0(4)$ can be qualitatively understood on the basis on inter- and intraband splittings of Δ_5 - Δ_1 transitions. Considerations of interband effects alone are not sufficient to explain the stress dependence of these structures since on this basis one would expect to observe one peak for parallel polarization and two peaks for perpendicular polarization, the energy of the former peak corresponding to one of the two components of the doublet $E'_0(2a)$ and $E'_0(2b)$. An inspection of Figs. 27(c), 27(d), 28(b), and 28(c) shows that this is not the case. However, if intraband effects are included, the transition which is allowed for the parallel polarization will occur at an energy between those of the perpendicular polarization doublet, thus accounting for the behavior of $E'_0(4b)$. We have not been able to understand the stress dependence of $E'_0(1)$ and $E'_0(4a)$ on the basis of the above considerations.

The strong polarization dependence of the E'_0 peaks for [111] stress can also be qualitatively explained on the basis of intraband splittings of Δ_5 . For $X \approx 90 \times 10^9$ dyn cm⁻² this splitting should be ≈ 20 –30 meV, which can just about be observed experimentally. However, the ratio α is approximately unity for this value of the intraband splitting and hence large polarization effects should be expected.

It is also evident that the applied electric field plays an important role in the observed effects. This is particularly true in the case of [110] stress for which a splitting of E'_0 is observed for light and electric field incident on a [001] face while for a $[1\bar{1}0]$ face only polarization effects are seen. We have attempted to analyze the effects of the electric field on the electroreflectance spectrum of the different samples investigated using the Aspnes' theory²⁴ but have not been able to make a self-consistent symmetry assignment on this basis.

Note added in proof. We have recently been informed by Dr. John Hensel of the Bell Telephone Labs in Murray Hill, N. J. of a revised value of $d = -4.44 \pm 0.30$ eV.

ACKNOWLEDGMENTS

We wish to express our thanks to Dr. M. Nathan of IBM for having supplied us with the GaAs samples used in this experiment. R. Stanford and A. P. Smith III, Brown University undergraduates, assisted with the measurements. The authors have benefitted from discussions with Professor J. C. Phillips, Professor M. L. Cohen, Dr. F. Herman, Dr. E. O. Kane, and Dr. T. Bergstresser.

APPENDIX A: E_0 AND $E_0 + \Delta_0$ PEAKS

1. Stress Parallel to [001]

From Eqs. (3) and (4) and perturbation theory, the wavefunctions of the valence band states at $\mathbf{k}=0$, to first order in α_0 , have been calculated to be

$$\begin{aligned} u_{v2,X} &= \left| \frac{3}{2}, \frac{3}{2} \right\rangle_{001}, \\ u_{v1,X} &= \left| \frac{3}{2}, \frac{3}{2} \right\rangle_{001} + \frac{1}{\sqrt{2}} \alpha_0 \left| \frac{1}{2}, \frac{1}{2} \right\rangle_{001}, \\ u_{v3,X} &= \left| \frac{1}{2}, \frac{1}{2} \right\rangle_{001} - \frac{1}{\sqrt{2}} \alpha_0 \left| \frac{3}{2}, \frac{3}{2} \right\rangle_{001}. \end{aligned} \quad (\text{A1})$$

It has been shown that the intensity of optical transitions is proportional to

$$|\langle \psi_1 | \hat{\epsilon} \cdot \mathbf{p} | \psi_2 \rangle|^2, \quad (\text{A2})$$

where $\hat{\epsilon}$ is the unit polarization vector of the electric field of the incident radiation and \mathbf{p} is the linear momentum.

From symmetry considerations⁴¹ it can be shown that the only nonzero matrix elements of \mathbf{p} between $\Gamma_{25'}$ (Γ_{15}) and $\Gamma_{2'}$ (Γ_1) are

$$P = \langle X \uparrow | p_x | S \uparrow \rangle = \langle Y \uparrow | p_y | S \uparrow \rangle = \langle Z \uparrow | p_z | S \uparrow \rangle \quad (\text{A3})$$

with similar expressions for spin down.

Equation (7) then follows from Eqs. (A1), (A2), and (A3) with

$$\begin{aligned} I_2^{11}(0) &= 0, & I_2^{12}(0) &\propto \frac{1}{2} P^2, \\ I_1^{11}(0) &\propto \frac{2}{3} P^2, & I_2^{21}(0) &\propto \frac{1}{6} P^2, \\ I_3^{11}(0) &\propto \frac{1}{3} P^2, & I_3^{21}(0) &\propto \frac{1}{3} P^2. \end{aligned} \quad (\text{A4})$$

2. Stress Parallel to [111]

For this stress direction it is convenient to make a rotation so that the [111] direction becomes the z axis. The wave functions of the valence band then have the form

$$\begin{aligned} \left| \frac{3}{2}, \frac{3}{2} \right\rangle_{111} &= \left| \left(\frac{1}{2} \right)^{1/2} (\bar{X} + i\bar{Y}) \uparrow \right\rangle, \\ \left| \frac{3}{2}, \frac{1}{2} \right\rangle_{111} &= \left| \left(\frac{1}{6} \right)^{1/2} [2\bar{Z} \uparrow + (\bar{X} + i\bar{Y}) \downarrow] \right\rangle, \\ \left| \frac{1}{2}, \frac{1}{2} \right\rangle_{111} &= \left| \left(\frac{1}{3} \right)^{1/2} [\bar{Z} \uparrow - (\bar{X} - i\bar{Y}) \downarrow] \right\rangle, \end{aligned} \quad (\text{A5})$$

⁴¹ See, e.g., G. Dresselhaus, A. F. Kip, and C. Kittel, *Phys. Rev.* **98**, 368 (1955); E. O. Kane, *Physics of III-V Compounds*, edited by R. K. Willardson and A. C. Beer (Academic Press Inc., New York, 1966), Vol. 1, p. 75.

where

$$\begin{aligned} \bar{X} &= \left(\frac{1}{2} \right)^{1/2} (X - Y), \\ \bar{Y} &= \left(\frac{1}{6} \right)^{1/2} (X + Y - 2Z), \\ \bar{Z} &= \left(\frac{1}{3} \right)^{1/2} (X + Y + Z). \end{aligned}$$

The stress-dependent wave functions have the same form as Eq. (A1) with α_0 replaced by α_1 .

3. Stress Parallel to [110]

For this stress direction it is convenient to make the transformation

$$\begin{aligned} \bar{X} &= Z, \\ \bar{Y} &= \left(\frac{1}{2} \right)^{1/2} (X - Y), \\ \bar{Z} &= \left(\frac{1}{2} \right)^{1/2} (X + Y), \end{aligned} \quad (\text{A6})$$

and hence the zero-stress wave functions become

$$\begin{aligned} \left| \frac{3}{2}, \frac{3}{2} \right\rangle_{110} &= \left| \left(\frac{1}{2} \right)^{1/2} (\bar{X} + i\bar{Y}) \uparrow \right\rangle, \\ \left| \frac{3}{2}, -\frac{1}{2} \right\rangle_{110} &= \left| \left(\frac{1}{6} \right)^{1/2} [2\bar{Z} \downarrow - (\bar{X} - i\bar{Y}) \uparrow] \right\rangle, \\ \left| \frac{1}{2}, -\frac{1}{2} \right\rangle_{110} &= \left| \left(\frac{1}{3} \right)^{1/2} [\bar{Z} \downarrow + (\bar{X} - i\bar{Y}) \uparrow] \right\rangle. \end{aligned} \quad (\text{A7})$$

The stress-dependent wave functions are obtained by first diagonalizing the 4×4 matrix in the upper left-hand corner of Eq. (12) and including the effects of the $|\frac{1}{2}, -\frac{1}{2}\rangle_{110}$ band by perturbation theory. This procedure yields

$$\begin{aligned} \bar{u}_{v2,X} &= \beta \left| \frac{3}{2}, \frac{3}{2} \right\rangle_{110} + \gamma \left| \frac{3}{2}, -\frac{1}{2} \right\rangle_{110} + \sqrt{2} \eta / \Delta_0 \left| \frac{1}{2}, -\frac{1}{2} \right\rangle_{110}, \\ \bar{u}_{v1,X} &= \beta \left| \frac{3}{2}, -\frac{1}{2} \right\rangle_{110} - \gamma \left| \frac{3}{2}, \frac{3}{2} \right\rangle_{110} + \alpha_0^{11} / \sqrt{2} \left| \frac{1}{2}, -\frac{1}{2} \right\rangle_{110}, \\ \bar{u}_{v3,X} &= \left| \frac{1}{2}, -\frac{1}{2} \right\rangle_{110} - \alpha_0^{11} / \sqrt{2} \left| \frac{3}{2}, -\frac{1}{2} \right\rangle_{110} - \sqrt{2} \eta / \Delta_0 \left| \frac{3}{2}, \frac{3}{2} \right\rangle_{110}. \end{aligned} \quad (\text{A8})$$

The stress-dependent intensities of Eq. (14) have been derived from Eqs. (A2), (A3), and (A8) with the result

$$I_2^{11}(0) \propto \frac{1}{3} P^2, \quad I_2^{12}(0) \propto P^2 / 2. \quad (\text{A9})$$

The expressions for the other zero-stress intensities are the same as in Eq. (A4).

APPENDIX B: E_1 AND $E_1 + \Delta_1$ PEAKS

1. Stress Parallel to [001]

The $\mathbf{k} \cdot \mathbf{p}$ band calculations for Ge and GaAs indicate that the approximate conduction and valence-band wavefunctions at the M_1 critical point in the [111] direction are

$$\begin{aligned} \bar{u}_{c,0} &= A |S \uparrow\rangle + B |\bar{z} \uparrow\rangle, \\ \bar{u}_{v1,0} &= \left| \frac{1}{2} \right)^{1/2} (\bar{X} + i\bar{Y}) \uparrow \rangle, \\ \bar{u}_{v2,0} &= \left| \frac{1}{2} \right)^{1/2} (\bar{X} - i\bar{Y}) \uparrow \rangle, \end{aligned} \quad (\text{B1})$$

where \bar{z} is the projection of the Γ_{15} conduction band (see Fig. 12) along the [111] direction. There are similar expressions for the $[1\bar{1}\bar{1}]$, $[\bar{1}1\bar{1}]$, and $[\bar{1}\bar{1}1]$ directions. For Ge $A = -0.60$ $B = +0.67$ and for GaAs $A = -0.56$ and $B = +0.56$.

The Hamiltonian matrix of Eq. (16) is obtained from Eqs. (2a) and (B1). The stress-dependent wavefunc-

tions for the Λ_3 valence bands, to first order in α_1 , are then calculated to be

$$\begin{aligned}\bar{u}_{v1,X} &= \bar{u}_{v1,0} - \frac{1}{2}\alpha_1 \bar{u}_{v2,0}, \\ \bar{u}_{v2,X} &= \bar{u}_{v2,0} + \frac{1}{2}\alpha_1 \bar{u}_{v1,0}.\end{aligned}\quad (\text{B2})$$

From symmetry considerations it can be shown that⁴¹

$$\begin{aligned}Q &= \langle X \uparrow | p_y | z \uparrow \rangle = \langle X \uparrow | p_z | y \uparrow \rangle, \\ &= \langle Y \uparrow | p_x | z \uparrow \rangle = \langle Y \uparrow | p_z | x \uparrow \rangle, \\ &= \langle Z \uparrow | p_x | y \uparrow \rangle = \langle Z \uparrow | p_y | x \uparrow \rangle,\end{aligned}\quad (\text{B3})$$

with similar expressions for spin down. All other matrix elements between $\Gamma_{25'}$ and Γ_{15} are zero.

The stress-independent intensities of Eq. (21) have been determined from Eqs. (A2), (A3), (B1), (B2), and (B3) with

$$\begin{aligned}I_{E_1^{11}}(0) &= I_{E_1+\Delta_1^{11}}(0) \\ &= I_{E_1^{\perp}}(0) = I_{E_1+\Delta_1^{\perp}}(0) \propto 4(AP/\sqrt{3} - \frac{1}{3}BQ)^2.\end{aligned}\quad (\text{B4})$$

In the following discussion all intensities will be given in units of $(AP/\sqrt{3} - \frac{1}{3}BQ)^2$.

2. Stress Parallel to $[\bar{1}\bar{1}\bar{1}]$

A. $[\bar{1}\bar{1}\bar{1}]$ Bands

The conduction and valence-band wavefunctions at the M_1 critical point in the $[\bar{1}\bar{1}\bar{1}]$ direction are given by Eq. (B1). The Hamiltonian matrix of Eq. (23) has been obtained from Eqs. (8) and (B1). Since there is no intraband splitting of these bands for $[\bar{1}\bar{1}\bar{1}]$ stress, the wavefunctions and intensities are not stress dependent [see Eq. (26)].

B. Bands along $[\bar{1}\bar{1}\bar{1}]$, $[\bar{1}\bar{1}\bar{1}]$, and $[\bar{1}\bar{1}\bar{1}]$

The wavefunctions at the $[\bar{1}\bar{1}\bar{1}]$ critical point may be written as

$$\begin{aligned}\bar{u}_{c,0'} &= A | S \uparrow \rangle + B | \bar{z}' \uparrow \rangle, \\ \bar{u}_{v1,0'} &= | (\frac{1}{2})^{1/2} (\bar{X}' + i\bar{Y}') \uparrow \rangle, \\ \bar{u}_{v2,0'} &= | (\frac{1}{2})^{1/2} (\bar{X}' - i\bar{Y}') \uparrow \rangle,\end{aligned}\quad (\text{B5})$$

where

$$\begin{aligned}\bar{z}' &= (\frac{1}{3})^{1/2}(x-y-z), \\ \bar{X}' &= (\frac{1}{2})^{1/2}(X+Y), \\ \bar{Y}' &= (\frac{1}{6})^{1/2}(X-Y+2Z).\end{aligned}\quad (\text{B6})$$

Equation (27) has been obtained from Eqs. (8) and (B6). The term $B^2\delta E_{111}'$ which appears in Eqs. (23),

(27), and (30) actually comes from $\langle \bar{u}_{c,0} | H_c | \bar{u}_{c,0} \rangle$ and hence can be included in the diagonal terms for the valence band states. The stress-dependent wavefunctions are then calculated to be, to first order in α_1' ,

$$\begin{aligned}\bar{u}_{v1,X'} &= \bar{u}_{v1,0'} + \frac{2}{3}\alpha_1' \bar{u}_{v2,0'}, \\ \bar{u}_{v2,X'} &= \bar{u}_{v2,0'} - \frac{2}{3}\alpha_1' \bar{u}_{v1,0'}.\end{aligned}\quad (\text{B7})$$

From Eqs. (A2), (A3), (B3), (B5), and (B7) the stress-dependent intensities of Eq. (29) have been determined with

$$\begin{aligned}I_{E_1^{11}}(0) &= I_{E_1+\Delta_1^{11}}(0) \propto 4, \\ I_{E_1^{\perp}}(0) &= I_{E_1+\Delta_1^{\perp}}(0) \propto \frac{5}{2}.\end{aligned}\quad (\text{B8})$$

3. Stress Parallel to $[\bar{1}\bar{1}\bar{1}]$

The Hamiltonian matrix of Eq. (30) is obtained from Eqs. (11), (B1), and (B5). For the bands along $[\bar{1}\bar{1}\bar{1}]$ and $[\bar{1}\bar{1}\bar{1}]$ the stress-dependent wavefunctions are

$$\begin{aligned}\bar{u}_{v1,X} &= \bar{u}_{v1,0} + \frac{1}{4}\alpha_1'' \bar{u}_{v2,0}, \\ \bar{u}_{v2,X} &= \bar{u}_{v2,0} - \frac{1}{4}\alpha_1'' \bar{u}_{v1,0}.\end{aligned}\quad (\text{B9})$$

While for the $[\bar{1}\bar{1}\bar{1}]$ and $[\bar{1}\bar{1}\bar{1}]$ we obtain

$$\begin{aligned}\bar{u}_{v1,X'} &= \bar{u}_{v1,0'} - \frac{1}{4}\alpha_1'' \bar{u}_{v2,0'}, \\ \bar{u}_{v2,X'} &= \bar{u}_{v2,0'} + \frac{1}{4}\alpha_1'' \bar{u}_{v1,0'}.\end{aligned}\quad (\text{B10})$$

The stress-dependent intensities [Eqs. (32) and (33)] have been calculated from Eqs. (A2), (A3), (B1), (B3), (B5), (B9), and (B10). For light incident on either $[001]$ or $[\bar{1}\bar{1}\bar{1}]$ face we find that

$$I_{E_1^{11}}(0) = I_{E_1+\Delta_1^{11}}(0) \propto 1$$

for the $[\bar{1}\bar{1}\bar{1}]$ and $[\bar{1}\bar{1}\bar{1}]$ bands, while

$$I_{E_1^{11}}(0) = I_{E_1+\Delta_1^{11}}(0) \propto 3$$

for the transitions between the $[\bar{1}\bar{1}\bar{1}]$ and $[\bar{1}\bar{1}\bar{1}]$ bands.

For the case of a $[001]$ face for perpendicular polarization we find that

$$I_{E_1^{\perp}}(0) = I_{E_1+\Delta_1^{\perp}}(0) \propto 3$$

for the $[\bar{1}\bar{1}\bar{1}]$ and $[\bar{1}\bar{1}\bar{1}]$ transitions and

$$I_{E_1^{\perp}}(0) = I_{E_1+\Delta_1^{\perp}}(0) \propto 1$$

for the other Λ transitions.

For light incident on a $[\bar{1}\bar{1}\bar{0}]$ face the perpendicular polarization intensity is equal to 2 for all bands.